Sample, estimate, aggregate:
A recipe for causal discovery foundation models

Anonymous authors
Paper under double-blind review

Abstract

Causal discovery, the task of inferring causal structure from data, has the potential to uncover mechanistic insights from biological experiments, especially those involving perturbations. However, causal discovery algorithms over larger sets of variables tend to be brittle against misspecification or when data are limited. For example, single-cell transcriptomics measures thousands of genes, but the nature of their relationships is not known, and there may be as few as tens of cells per intervention setting. To mitigate these challenges, we propose a foundation model-inspired approach: a supervised model trained on large-scale, synthetic data to predict causal graphs from summary statistics — like the outputs of classical causal discovery algorithms run over subsets of variables and other statistical hints like inverse covariance. Our approach is enabled by the observation that typical errors in the outputs of classical methods remain comparable across datasets. Theoretically, we show that the model architecture is well-specified in terms of computational capacity. Empirically, we train the model to be robust to misspecification and distribution shift using diverse datasets. Experiments on biological and synthetic data confirm that this model generalizes well beyond its training set, runs on graphs with hundreds of variables in seconds, and can be adapted (zero-shot or finetuned) to different underlying data assumptions.[1]

1 Introduction

A fundamental aspect of scientific research is to discover and validate causal hypotheses involving variables of interest. Given observations of these variables, the goal of causal discovery algorithms is to extract such hypotheses in the form of directed graphs, in which edges denote causal relationships (Spirtes et al., 2001). There are several challenges to their widespread adoption in basic science. The core issue is that the correctness of these algorithms is tied to their assumptions on the data-generating processes, which are unknown in real applications. In principle, one could circumvent this issue by exhaustively running discovery algorithms with different assumptions and comparing their outputs with surrogate measures that reflect graph quality (Faller et al., 2023). However, this search would be costly: current algorithms must be optimized from scratch each time, and they scale poorly to the graph and dataset sizes present in modern scientific big data (Replogle et al., 2022).

Causal discovery algorithms follow two primary approaches that differ in their treatment of the causal graph. Discrete optimization algorithms explore the super-exponential space of graphs by proposing and evaluating changes to a working graph (Glymour et al., 2019). While these methods are fast on small graphs, the combinatorial space renders them intractable for exploring larger structures. Furthermore, these algorithms are driven by hypothesis tests, which necessarily impose functional assumptions on the data-generating process, and whose results can be erroneous, especially as the number of variables increases. An alternative is to frame causal discovery as a continuous optimization over weighted adjacency matrices. These algorithms either fit a generative model to the data and extract the causal graph as a parameter (Zheng et al., 2018), or train a supervised learning model on simulated data (Lorch et al., 2022). However, the former must be trained from scratch per-dataset, and latter are not easily extensible to causal mechanisms beyond those in the training set.

---

[1] Our code is available in the supplement.

In this work, we present SEA: Sample, Estimate, Aggregate, a supervised causal discovery framework that aims to perform well even when data-generating processes are unknown, and to easily incorporate prior knowledge when it is available. We train a deep learning model to predict causal graphs from two types of statistical descriptors: the estimates of classical discovery algorithms over small subsets, and graph-level statistics. Classical discovery algorithms output a representation of a graph's equivalency class, whose format is largely consistent across algorithms, and whose errors are comparable across datasets. Statistics like correlation or inverse covariance are strong indicators for a graph's overall connectivity and can reduce the number of subsets on which we must run discovery algorithms. Theoretically, we show that our model can implement a combinatorial algorithm that recovers larger causal graphs that are consistent with smaller, marginal subgraphs. Empirically, our training procedure forces the model to predict causal graphs across diverse synthetic data, including on datasets that are misaligned with the discovery algorithms' assumptions, or when insufficient subsets are provided.

Our experiments probe three qualities that we view a foundation model should fulfill, with thorough comparison to three classical baselines and five deep learning approaches. Specifically, we assess the framework's ability to generalize to unseen and out-of-distribution data; to steer predictions based on prior knowledge; and to perform well in low-data regimes. SEA attains the state-of-the-art results on synthetic and real causal discovery tasks, while providing 10-1000x faster inference. To incorporate domain knowledge, we show that it is possible to swap classic discovery algorithms at inference time, for significant improvements on datasets that match the assumptions of the new algorithm. Our models can also be finetuned at a fraction of the training cost to accommodate new graph-level statistics that capture different (e.g. nonlinear) relationships. We extensively analyze SEA in terms of low-data performance, scalability, causal identifiability, and other design choices. To conclude, while our experiments focus on specific algorithms and architectures, this work presents a blueprint for designing causal discovery foundation models, in which sampling heuristics, classical causal discovery algorithms, and summary statistics are the fundamental building blocks.

2 Background and related work

2.1 Causal structure learning

A **causal graphical model** is a directed, acyclic graph $G = (V, E)$, where each node $i \in V$ corresponds to a random variable $X_i \in X$ and each edge $(i, j) \in E$ represents a causal relationship from $X_i \to X_j$. There are a number of assumptions that relate data distribution P_X to G (Spirtes et al., 2001; Hauser & Bühlmann, 2012), which determine whether G is identifiable Causal graphical models allow us to perform *interventions* on nodes i by setting conditional $P(X_i \mid X_{\pi_i})$ to a different distribution $\tilde{P}(X_i \mid X_{\pi_i})$. In this paper, our experiments cover the observational case (no interventions) and the case with perfect interventions on each node, i.e. $\tilde{P}(X_i \mid X_{\pi_i}) = \tilde{P}(X_i)$.

Given a dataset $D \sim P_X$, the goal of **causal structure learning** (causal discovery) is to recover G. There are two main challenges. First, the number of possible graphs is super-exponential in the number of nodes N, so algorithms must navigate this combinatorial search space efficiently. Second, depending on data availability and the underlying data generation process, causal discovery algorithms may or may not be able to recover G in practice. In fact, many algorithms are only analyzed in the infinite-data regime and require at least thousands of data samples for reasonable empirical performance (Spirtes et al., 2001; Brouillard et al., 2020).

Discrete optimization methods make atomic changes to a proposal graph until a stopping criterion is met. Constraint-based algorithms identify edges based on conditional independence tests, and their correctness is inseparable from the empirical results of those tests (Glymour et al., 2019), whose statistical power depends directly on dataset size. These include the observational FCI and PC algorithms (Spirtes et al., 1995), and the interventional JCI algorithm (Mooij et al., 2020). Score-based methods also make iterative modifications to a working graph, but their goal is to maximize a continuous score over the discrete space of all valid graphs, with the true graph at the optimum. Due to the intractable search space, these methods often make decisions based on greedy heuristics. Classic examples include GES (Chickering, 2002), GIES (Hauser & Bühlmann, 2012), CAM (Bühlmann et al., 2014), LiNGAM (Shimizu et al., 2006), and IGSP (Wang et al., 2017).

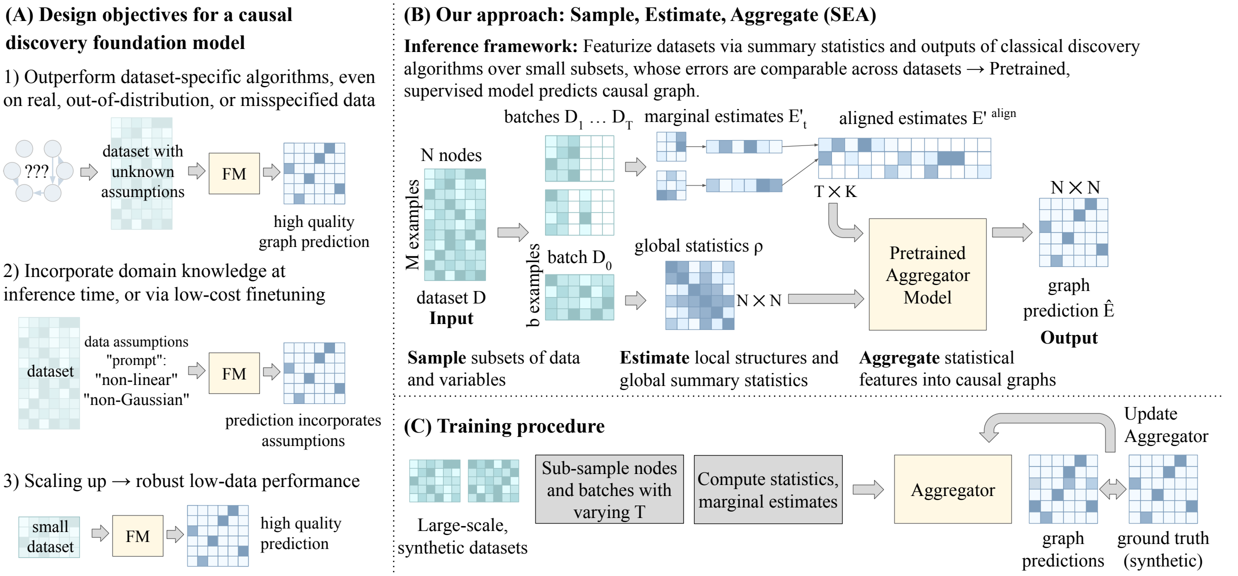
(A) Design objectives for a causal discovery foundation model
1) Outperform dataset-specific algorithms, even on real, out-of-distribution, or misspecified data
???
dataset with unknown assumptions
FM
high quality graph prediction
2) Incorporate domain knowledge at inference time, or via low-cost finetuning
dataset
data assumptions "prompt": "non-linear" "non-Gaussian"
FM
prediction incorporates assumptions
3) Scaling up → robust low-data performance
small dataset
FM
high quality prediction
(B) Our approach: Sample, Estimate, Aggregate (SEA)
Inference framework: Featurize datasets via summary statistics and outputs of classical discovery algorithms over small subsets, whose errors are comparable across datasets → Pretrained, supervised model predicts causal graph.
N nodes
M examples
dataset D
Input
batches D_1 … D_T
b examples
batch D_0
marginal estimates E'_t
aligned estimates E'^{align}
T × K
global statistics ρ
N × N
Pretrained Aggregator Model
N × N
graph prediction $\hat{E}$
Output
Sample subsets of data and variables
Estimate local structures and global summary statistics
Aggregate statistical features into causal graphs
(C) Training procedure
Large-scale, synthetic datasets
Sub-sample nodes and batches with varying T
Compute statistics, marginal estimates
Aggregator
Update Aggregator
graph predictions
ground truth (synthetic)

Figure 1: Overview of our goals and approach. (A) Criteria we aim to fulfill. (B-C) Inference and training procedure. Green: raw data. Blue: graph / features. Yellow: Learned. Gray: Stochastic, but not learned.

Continuous optimization approaches recast the combinatorial space of graphs into a continuous space of weighted adjacency matrices. Many of these works train a generative model to learn the empirical data distribution, which is parameterized through the adjacency matrix (Zheng et al., 2018; Lachapelle et al., 2020; Brouillard et al., 2020). Others focus on properties related to the empirical data distribution, such as a relationship between the underlying graph and the Jacobian of the learned model (Reizinger et al., 2023), or between the Hessian of the data log-likelihood and the topological order (Sanchez et al., 2023). Finally, most similar to this work, amortized inference approaches (Ke et al., 2022; Lorch et al., 2022) frame causal discovery as a supervised learning problem of predicting (synthetic) graphs from (synthetic) datasets. However, to incorporate new information, they must simulate new datasets and re-train the models. Since they operate on raw observations, they also scale poorly to larger datasets.

2.2 Foundation models

The concept of foundation models has revolutionized the machine learning workflow in a variety of disciplines: instead of training domain-specific models from scratch, we start from a pretrained, general-purpose model (Bommasani et al., 2021). This work describes a blueprint for designing "foundation models" in the context of causal discovery. The precise definition of a foundation model varies by application, but we aim to fulfill the following properties (Figure 1A), enjoyed by modern text and image foundation models (Radford et al., 2021; Brown et al., 2020).

1. A foundation model should enable us to outperform domain-specific models trained from scratch, even if the former has never seen similar tasks during training (Radford et al., 2019). In the context of causal discovery, we would like to train a model that outperforms any individual algorithm on real, misspecified, and/or out-of-distribution datasets.
2. It should be possible to explicitly steer a foundation model's behavior towards better performance on new tasks, either directly at inference time, e.g. "prompting" (Reynolds & McDonell, 2021), or at low cost compared to pretraining (Ouyang et al., 2022). Here, we would like to easily change our causal discovery algorithm's "assumptions" regarding the data, e.g. by incorporating the knowledge of non-linearity, non-Gaussianity.
3. Scaling up a foundation model should lead to improved performance in few-shot or data-poor regimes (Brown et al., 2020). This aspect we analyze empirically.

In the following sections, we will revisit these desiderata from both the design and experimental perspectives.

3 Methods

3.1 Inference procedure

Sea is a causal discovery framework that learns to resolve statistical features and estimates of marginal graphs into a global causal graph. The inference procedure is depicted in Figure 1B. Specifically, given a new dataset $D \in \mathbb{R}^{M\times N}$ faithful to graph $G = (V, E)$, we apply the following stages.

Sample: takes as input dataset D; and outputs data batches $\{D_0, D_1, \ldots, D_T\}$ and node subsets $\{S_1, \ldots, S_T\}$.

1. Sample $T + 1$ batches of $b \ll M$ observations uniformly at random from D.
2. Compute selection scores $\alpha \in (0, 1)^{N\times N}$ over D_0 (e.g. correlation or inverse covariance).
3. Sample T node subsets of size k. Each subset $S_t \subseteq V$ is constructed iteratively, where nodes are added with probability proportional to $\sum_{j\in S_t} \alpha_{i,j}$ (details and alternatives in B.6).

Estimate: takes as inputs data batches, node subsets, and (optionally) intervention targets; and outputs global statistics ρ and marginal estimates $\{E'_1, \ldots, E'_T\}$.

1. Compute global statistics $\rho \in \mathbb{R}^{N\times N}$ over D_0 (e.g. correlation or inverse covariance).
2. Run discovery algorithm f to obtain marginal estimates $f(D_t[S_t]) = E'_t$ for $t = 1 \ldots T$.

We use $D_t[S_t]$ to denote the observations in D_t that correspond only to the variables in S_t. Each estimate E'_t is a $k \times k$ adjacency matrix, corresponding to the k nodes in S_t.

Aggregate: takes as inputs global statistics, marginal estimates, and node subsets. A pretrained aggregator model outputs the predicted global causal graph $\hat{E} \in (0, 1)^{N\times N}$ (Section 3.3).

3.2 Training procedure

The training procedure mirrors the inference procedure (Figure 1C). Each input is a whole dataset (summarized into global statistics and a set of marginal estimates), and the supervised output is the ground truth graph. Sampling and estimation are run in parallel on CPU, while aggregation is run on GPU.

We trained two aggregator models, which employed the Fci algorithm with the Fisherz test and Gies algorithm with the Bayesian information criterion (Schwarz, 1978). Both estimation algorithms were chosen for speed, and they differ in the types of edges they output (e.g. Fci reports ancestral relations). Note that the algorithm used for inference can differ from the one used during training, as long as their outputs are the same format, e.g. a CPDAG (Andersson et al., 1997) (experiments in Section 5.2). The training dataset contains both data that are correctly and incorrectly specified (details in Section 4.1), so the aggregator is forced to predict the correct graph regardless. In addition, each training instance is provided a random number of marginal estimates, which might not cover every edge. As a result, the aggregator must extrapolate to unseen edges using the available estimates and the global statistics. For example, if two variables have low correlation, and they are located in different neighborhoods of the already-identified graph, it may be reasonable to assume that they are unconnected.

3.3 Model architecture

The aggregator is a neural network that takes as input: global statistics $\rho \in \mathbb{R}^{N\times N}$, marginal estimates $E'_{1\ldots T} \in \mathcal{E}^{T\times k\times k}$, and node subsets $S_{1\ldots T} \in [N]^{T\times k}$ (Figure 2), where $\mathcal{E}$ is the set of output edge types for the causal discovery algorithm f.[2]

We project global statistics into the model dimension via a learned linear projection matrix $W_\rho : \mathbb{R} \to \mathbb{R}^d$, and we embed edge types via a learned embedding $\text{ebd}_{\mathcal{E}} : \mathcal{E} \to \mathbb{R}^d$. To collect estimates of the same edge over all subsets, we align entries of $E'_{1\ldots T}$ into $E_T^{'\text{align}} \in \mathcal{E}^{T\times K}$

$$E_{t,e=(i,j)}^{'\text{align}} = \begin{cases} E'_{t,i,j} & \text{if } i \in S_t, j \in S_t \\ 0 & \text{otherwise} \end{cases} \tag{1}$$

---

[2] E.g. "no relationship," "X causes Y," "X is not a descendent of Y"

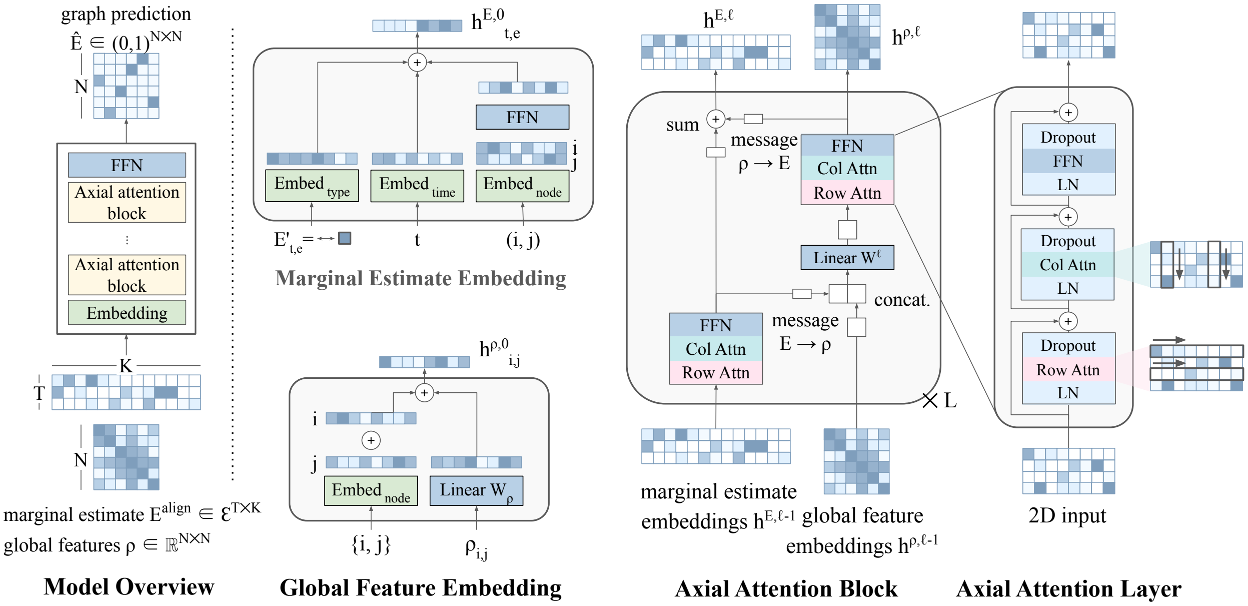

Figure 2: Aggregator architecture. Marginal graph estimates and global statistics are embedded into the model dimension. 1D positional embeddings are added along both rows and columns. Embedded features pass through a series of axial attention blocks, which attend to the marginal and global features. Final layer global features pass through a feedforward network to predict the causal graph.

where t indexes into the subsets, e indexes into the set of unique edges, and K is the number of unique edges. We add learned 1D positional embeddings along both dimensions of each input,

$$\begin{aligned}\text{pos-ebd}(\rho_{i,j}) &= \text{ebd}_{\text{node}}(i') + \text{ebd}_{\text{node}}(j') \\ \text{pos-ebd}(E'^{\text{align}}_{t,e}) &= \text{ebd}_{\text{time}}(t) + \text{FFN}([\text{ebd}_{\text{node}}(i'), \text{ebd}_{\text{node}}(j')])\end{aligned}$$

where i', j' index into a random permutation on V for invariance to node permutation and graph size.[3] Due to the (a)symmetries of their inputs, pos-ebd$(\rho_{i,j})$ is symmetric, while pos-ebd$(E'^{\text{align}}_{t,e})$ considers the node ordering. In summary, the inputs to our axial attention blocks are

$$h^{\rho}_{i,j} = (W_\rho \rho)_{i,j} + \text{pos-ebd}(\rho_{i,j}) \tag{2}$$

$$h^{E}_{t,e} = \text{ebd}_{\mathcal{E}}(E'^{\text{align}}_{t,e}) + \text{pos-ebd}(E'^{\text{align}}_{t,e}) \tag{3}$$

for $i, j \in [N]^2$, $t \in [T]$, $e \in [K]$. Note that attention is permutation invariant, so positional embeddings are *required* for the model to know which edges belong to the same subset, or what each edge's endpoints endpoints are.

Axial attention An axial attention block contains two axial attention layers (marginal estimates, global statistics) and a feed-forward network (Figure 2, right). Given a 2D input, an axial attention layer attends first along the rows, then along the columns. For example, on a matrix of size `(R,C,d)`, one pass of the axial attention layer is equivalent to running standard self-attention along `C` with batch size `R`, followed by the reverse. For marginal estimates, `R` is the number of subsets T, and `C` is the number of unique edges K. For global statistics, `R` and `C` are both the total number of vertices N.

Following Rao et al. (2021), each self-attention mechanism is preceded by layer normalization and followed by dropout, with residual connections to the input,

$$x = x + \text{Dropout}(\text{Attn}(\text{LayerNorm}(x))). \tag{4}$$

---

[3] The random permutation $i' = \sigma(V)_i$ allows us to avoid updating positional embeddings of lower order positions more than higher order ones, due to the mixing of graph sizes during training.

We pass messages between the marginal and global layers to propagate information. Let $\phi_{E,\ell}$ be marginal layer ℓ, let $\phi_{\rho,\ell}$ be global layer ℓ, and let $h^{\cdot,\ell}$ denote the hidden representations out of layer ℓ. The marginal to global message $m^{E\to\rho} \in \mathbb{R}^{N\times N\times d}$ contains representations of each edge averaged over subsets,

$$m_{i,j}^{E\to\rho,\ell} = \begin{cases} \frac{1}{T_e}\sum_t h_{t,e=(i,j)}^{E,\ell} & \text{if } \exists S_t, i,j \in S_t \\ \epsilon & \text{otherwise.} \end{cases} \tag{5}$$

where T_e is the number of S_t containing e, and missing entries are padded to learned constant ϵ. The global to marginal message $m^{\rho\to E} \in \mathbb{R}^{K\times d}$ is simply the hidden representation itself,

$$m_{t,e=(i,j)}^{\rho\to E,\ell} = h_{i,j}^{\rho,\ell}. \tag{6}$$

We update representations based on these messages as follows.

$$h^{E,\ell} = \phi_{E,\ell}(h^{E,\ell-1}) \qquad \text{(marginal feature)} \tag{7}$$

$$h^{\rho,\ell-1} \leftarrow W^\ell \left[h^{\rho,\ell-1}, m^{E\to\rho,\ell}\right] \qquad \text{(marginal to global)} \tag{8}$$

$$h^{\rho,\ell} = \phi_{\rho,\ell}(h^{\rho,\ell-1}) \qquad \text{(global feature)} \tag{9}$$

$$h^{E,\ell} \leftarrow h^{E,\ell} + m^{\rho\to E,\ell} \qquad \text{(global to marginal)} \tag{10}$$

$W^\ell \in \mathbb{R}^{2d\times d}$ is a learned linear projection, and $[\cdot]$ denotes concatenation.

Graph prediction For each pair of vertices $i \neq j \in V$, we predict $e = 0, 1$, or 2 for no edge, $i \to j$, and $j \to i$. We do not additionally enforce that our predicted graphs are acyclic, similar in spirit to Lippe et al. (2022). Given the output of the final axial attention block h^ρ, we compute logits

$$z_{\{i,j\}} = \text{FFN}\left(\left[h_{i,j}^\rho, h_{j,i}^\rho\right]\right) \in \mathbb{R}^3 \tag{11}$$

which correspond to probabilities after softmax normalization. The overall output $\hat{E} \in \{0,1\}^{N\times N}$ is supervised by the ground truth E. Our model is trained with cross entropy loss and L2 regularization.

Implementation details Unless otherwise noted, inverse covariance is used for the global statistic and selection score, due to its relationship to partial correlation. We sample batches of size $b = 500$ over $k = 5$ nodes each (analysis in 5.4). Our model was implemented with 4 layers with 8 attention heads and hidden dimension 64. Our model was trained using the AdamW optimizer with a learning rate of 1e-4 (Loshchilov & Hutter, 2019). See B.3 for additional details about hyperparameters.

Complexity The aggregator should be be invariant to node labeling, while maintaining the order of sampled subsets, so attention-based architectures were a natural choice (Vaswani et al., 2017). If we concatenated ρ and $E'_{1\ldots T}$ into a length N^2T input, quadratic-scaling attention would cost $O(N^4T^2)$. Instead, we opted for axial attention blocks, which attend along each of the three axes separately in $O(N^3T + N^2T^2)$. Both are parallelizable on GPU, but the latter is more efficient, especially on larger N.

3.4 Theoretical interpretation

Marginal graph resolution It is well-established that estimates of causal graphs over subsets of variables can be "merged" into consistent graphs over their union (Faller et al., 2023), and various algorithms have been proposed towards this task (Tillman et al., 2008; Huang et al., 2020). Our main theoretical contribution is demonstrating that our axial attention model can implement such an algorithm under realistic conditions (description of algorithm and all proofs in Appendix A).

Theorem 3.1. *Let $G = (V, E)$ be a directed acyclic graph with maximum degree d. For $S \subseteq V$, let E'_S denote the marginal estimate over S. Let $\mathcal{S}_d$ denote the superset that contains all subsets $S \subseteq V$ of size at most d. Given $\{E'_S\}_{S\in\mathcal{S}_{d+2}}$, a stack of L axial attention blocks has the capacity to recover G's skeleton and v-structures in $O(N)$ width, and propagate orientations on paths of $O(L)$ length.*

There are two practical considerations that motivate a framework like Sea, instead of directly running these reconciliation algorithms. First, many of these algorithms rely on specific characterizations of the data-generating process, e.g. linear non-Gaussian (Huang et al., 2020). While our proof does not constrain the causal mechanisms or exogenous noise, it assumes that the marginal estimates are correct. These assumptions may not hold on real data. However, the failure modes of causal discovery algorithms may be similar across datasets and can be corrected using statistics that capture richer information. For example, an algorithm that assumes linearity will make (predictably) asymmetric mistakes on non-linear data and underestimate the presence of edges. However, we may be able to recover nonlinear relationships with statistics like distance correlation (Sz'ekely et al., 2007). By training a deep learning model to reconcile marginal estimates and interpret global statistics, we are less sensitive to artifacts of sampling and discretization (e.g. p-value thresholds, statistics $\lesseqgtr 0$). The second consideration is that checking a combinatorial number of subsets is wasteful on smaller graphs and infeasible on larger graphs. In fact, if we only leverage marginal estimates, we must check at least $O(N^2)$ subsets to cover each edge at least once. To this end, the classical Independence Graph algorithm (Spirtes et al., 2001) motivates statistics such as inverse covariance to initialize the undirected skeleton and reduce the number of independence tests required. This allows us to use marginal estimates more efficiently, towards answering orientation questions. We verify this latter consideration in Section 5.4, where we empirically quantify the number of estimates a global statistic is "worth."

On identifiability The goal of this paper is a principled, yet practical framework for causal discovery. Instead of focusing on the identifiability of any particular setting, we provide these interpretations of our model's outputs, and show empirically that our model respects classic identifiability theory (Section 5.3). When all assumptions are upheld, and infinite data are available, the model has the capacity to infer a sound graph, as far as its (Markov/interventional) equivalence class. In practice, the model will output an orientation for all edges, but the graph can be interpreted as one member of an equivalence class. When data do not match a causal discovery algorithm's assumptions, its performance is inherently an empirical question, and we show empirically that our model still does well (Section 5.1). Finally, recent work (Montagna et al., 2024) has specifically studied the identifiability of amortized causal discovery algorithms in depth, and their findings are complementary to our own.

4 Experimental setup

Our experiments aim to address the three desiderata proposed in Section 2.2 – namely, generalization, adaptability, and emergent few-shot behavior. These experiments span both real and synthetic data. Real experiments quantify the practical utility of this framework, while synthetic experiments allow us to probe and compare each design choice in a controlled setting.

4.1 Datasets

We pretrained Sea models on 6,480 synthetic datasets, which constitute approximately 280 million individual observations, each of 10-100 variables.[4] To assess generalization and robustness, we evaluate on unseen in-distribution and out-of-distribution synthetic datasets, as well as two real biological datasets (Sachs et al., 2005; Replogle et al., 2022), using the versions from Wang et al. (2017); Chevalley et al. (2022). To probe for emergent few-shot behavior, we down-sample both the training and testing sets. We also include experiments on simulated mRNA datasets with unseen datasets in Appendix C.2 (Dibaeinia & Sinha, 2020).

The training datasets were constructed by 1) sampling Erdős-Rényi and scale free graphs with $N = 10, 20, 100$ nodes and $E = N, 2N, 3N, 4N$ expected edges; 2) sampling random instantiations of causal mechanisms (Linear, NN with additive/non-additive Gaussian noise); and 3) iteratively sampling observations in topological order (details in Appendix B.1). For each graph, we generated both observational and interventional datasets with $1000N$ points, either all observational or split equally among observational and perfect single-node interventions. We generated 90 training, 5 validation, and 5 testing datasets for each combination. For testing,

---

[4] 3 mechanisms, 3 graph sizes, 4 sparsities, 2 topologies, $1000N$ examples, 90 datasets → 280,800,000 examples. For a sense of scale, single cell foundation models are trained on 300K (Rosen et al., 2024) to 30M cells (Cui et al., 2024).

we also sampled out-of-distribution datasets with 1) Sigmoid and Polynomial mechanisms with Gaussian noise; and 2) Linear with additive non-Gaussian noise.

4.2 Metrics

We report standard causal discovery metrics (Lorch et al., 2022), computed with respect to the ground truth graph. In the observational setting, the "oracle" value of each metric will vary depending on the size of the equivalence class (e.g. if multiple graphs are observationally equivalent, the expected accuracy is < 1; see Section 5.3 for more analysis). For all continuous metrics, we exclude the diagonal since several baselines manually set it to zero (Brouillard et al., 2020; Lopez et al., 2022).

SHD: Structural Hamming distance is the minimum number of edge edits required to match two graphs (Tsamardinos et al., 2006). Discretization thresholds are as published or default to 0.5.

mAP: Mean average precision computes the area under precision-recall curve per edge and averages over the graph. The random guessing baseline depends on the positive rate.

AUC: Area under the ROC curve (Bradley, 1997) computed per edge (binary prediction) and averaged over the graph. For each edge, 0.5 indicates random guessing, while 1 indicates perfect performance.

Orientation accuracy: We compute the accuracy of edge orientations as

$$\text{OA} = \frac{\sum_{(i,j)\in E} \mathbb{1}\{P(i,j) > P(j,i)\}}{\|E\|}. \tag{12}$$

Since OA is normalized by $\|E\|$, it is invariant to the positive rate. In contrast to orientation F1 (Geffner et al., 2022), it is also invariant to the assignment of forward/reverse edges as 1/0.

4.3 Baselines

We compare against several deep learning and classical baselines. All baselines were trained and/or run from scratch on each testing dataset using their published code and hyperparameters, except Avici (their recommended checkpoint was trained on their synthetic train and test sets after publication, Appendix B.2).

DCDI (Brouillard et al., 2020) extracts the causal graph as a parameter of a generative model. The G and Dsf variants use Gaussian or deep sigmoidal flow likelihoods, respectively. **DCD-FG** (Lopez et al., 2022) follows DCDI-G, but factorizes the graph into a product of two low-rank matrices for scalability. **DiffAn** (Sanchez et al., 2023) uses the trained model's Hessian to obtain a topological ordering, followed by a classical pruning algorithm. **AVICI** (Lorch et al., 2022) uses an amortized inference approach to estimate $P(G \mid D)$ over a class of data-generating mechanisms via variational inference. Both DCD-* and AVICI were run with full knowledge of intervention targets. **VarSort** (a.k.a. "sort and regress") (Reisach et al., 2021) sorts nodes by marginal variance and sparsely regresses nodes based on their predecessors. This naive baseline is intended to reveal artifacts of synthetic data generation. **FCI, GIES** run the FCI and GIES algorithms over *all* nodes. VarSort, Fci, and Gies were run using non-parametric bootstrapping (Friedman et al., 1999), with 100 subsets of 500 examples each.

5 Results

We highlight representative results in each section, with additional experiments and analyses in Appendix C.

1. Section 5.1 examines the case where we have no prior knowledge about the data. Our models achieve high performance out-of-the-box, even when the data are misspecified or out-of-domain.
2. Section 5.2 focuses on the case where we do know (or can estimate) the class of causal mechanisms or exogenous noise. We show that adapting our pretrained models with this information at zero/low cost leads to substantial improvement and exceeds the best baseline trained from scratch.
3. Section 5.3 analyzes Sea predictions in context of classic identifiability theory. In particular, we focus on the linear Gaussian case, and show that Sea approaches "oracle" performance (with respect to the MEC), while simply running a classic discovery algorithm cannot, on our finite datasets.

Table 1: Causal discovery on synthetic datasets. Mean/std over 5 distinct Erdős-Rényi graphs. † indicates o.o.d. setting. ∗ indicates non-parametric bootstrapping. Runtimes based on 1 CPU and 1 V100 GPU. Baseline implementation details in B.2. Additional baselines and ablations in Appendix C.

N	E	Model	Linear		NN add.		Sigmoid†		Polynomial†		Overall
			mAP ↑	SHD ↓	mAP ↑	SHD ↓	mAP ↑	SHD ↓	mAP ↑	SHD ↓	Time(s) ↓
20	20	Dcdi-G	0.59±.12	6.4±.9	0.78±.07	**3.0**±.7	0.36±.06	42.7±.3	0.42±.08	10.4±.4	4735.7
		Dcdi-Dsf	0.66±.16	5.2±.3	0.69±.18	4.2±.5	0.37±.04	43.2±.4	0.26±.08	15.7±.2	3569.1
		DiffAn	0.19±.09	40.2±4.4	0.16±.10	38.6±3.1	0.29±.11	19.2±.6	0.09±.03	49.7±4.6	434.3
		Avici	0.48±.17	17.2±.1	0.59±.09	10.8±.1	0.42±.13	17.2±.8	0.24±.08	18.4±.1	2.0
		VarSort*	0.81±.08	10.0±.4	0.81±.15	6.6±.7	0.50±.13	16.1±.7	0.33±.13	17.1±.1	0.4
		Fci*	0.66±.07	19.0±.3	0.42±.19	17.4±.2	0.56±.08	18.5±.5	0.41±.14	18.9±.3	22.2
		Gies*	0.84±.08	7.4±.0	0.79±.07	9.0±.1	0.71±.10	12.5±.7	0.62±.09	13.7±.7	482.1
		Sea (Fci)	**0.96**±.03	3.2±.6	0.91±.04	5.0±.8	**0.85**±.09	**6.7**±.1	**0.69**±.09	**9.8**±.2	4.2
		Sea (Gies)	**0.97**±.02	**3.0**±.9	**0.94**±.03	3.4±.4	0.84±.07	8.1±.8	**0.69**±.12	10.1±.9	3.0
100	400	Dcd-Fg	0.05±.00	3068±131	0.07±.00	3428±154	0.13±.02	3601±272	0.12±.03	3316±698	1838.2
		Avici	0.12±.02	391±8	0.17±.01	407±19	0.10±.02	398±11	0.03±.00	402±19	9.3
		VarSort*	0.80±.02	224±10	0.18±.03	1139±269	0.51±.05	350±15	0.27±.04	380±17	5.1
		Sea (Fci)	0.84±.02	162±12	0.04±.00	403±16	0.63±.03	247±17	0.34±.04	**325**±22	19.2
		Sea (Gies)	**0.91**±.01	**116**±7	**0.27**±.10	**364**±34	**0.69**±.03	**218**±21	**0.38**±.04	328±22	3.1

4. Section 5.4 contains a variety of ablation studies. In particular, Sea exhibits impressive low-data performance, requiring only 400 samples to perform well on $N = 100$ datasets. We also ablate estimation hyperparameters and the contribution of marginal/global features.

5.1 SEA generalizes to out-of-distribution, misspecified, and real datasets

Table 1 summarizes our controlled experiments on synthetic data. Sea exceeds all baselines in the Linear case, which matches the models' assumptions exactly (causal discovery algorithms and inverse covariance). In the misspecified (NN) or misspecified *and* out-of-distribution settings (Sigmoid, Polynomial), Sea also attains the best performance in the vast majority of cases, even though Dcdi and Avici both have access to the raw data. Furthermore, our models outperform VarSort in every single setting, while most baselines are unable to do so consistently. This indicates that our models do not simply overfit to spurious features of the synthetic data generation process.

Table 2 illustrates that we exceed baselines on single cell gene expression data from CausalBench (Chevalley et al., 2022; Replogle et al., 2022). Furthermore, when we increase the subset size to $b = 2000$, we achieve very high precision (0.838) over 2834 predicted edges. Sea runs within 5s on this dataset of 162k cells and $N = 622$ genes, while the fastest naive baseline takes 5 minutes and the slowest deep learning baseline takes 9 hours (run in parallel on subsets of genes).

5.2 SEA adapts to new data assumptions with zero to minimal finetuning

We illustrate two strategies that allow us to use pretrained Sea models with different implicit assumptions. First, if two causal discovery algorithms share the same output format, they can be used interchangeably for marginal estimation. On observational, linear *non*-Gaussian data, replacing the Ges algorithm with Lingam (Shimizu et al., 2006) is beneficial without any other change (Table 4). The same improvement can be observed on Polynomial and Sigmoid non-additive data, when running Fci with a polynomial kernel conditional independence test (Kci, Zhang et al. (2011)) instead of the Fisherz test, which assumes linearity (Table 5). In principle, different algorithms might make different mistakes, so this strategy could lead to out-of-distribution inputs for the pretrained aggregator. However, we find empirically (Table 7) that performance remains similar for multiple unseen discovery algorithms, even those of an entirely different class (permutation-based GRaSP (Lam et al., 2022), instead of constraint/score-based).

Table 2: Results on K562 single cell data, with STRING database (physical) as ground truth. Baselines taken from Chevalley et al. (2022).

Model	P ↑	R ↑	F1 ↑	Time(s) ↓
GRNboost	0.070	**0.710**	0.127	316
Gies	0.190	0.020	0.036	2350
NoTears	0.080	0.620	0.142	32883
Dcdi-G	0.180	0.030	0.051	16561
Dcdi-Dsf	0.140	0.040	0.062	5709
Dcd-Fg	0.110	0.070	0.086	6368
Sea (G)+Corr	0.491	0.109	**0.179**	**4**
with $b = 2000$	**0.838**	0.093	0.167	5

Table 3: Performance on Sachs (C.4) varies depending on implicit (Avici training set) and explicit (Sea variants) assumptions.

Model	mAP ↑	AUC ↑	SHD ↓
Dcdi-Dsf	0.20	0.59	20.0
Avici-L	0.35	0.78	20.0
Avici-R	0.29	0.65	18.0
Avici-L+R	**0.59**	**0.83**	14.0
Sea (F)	0.23	0.54	24.0
+Kci	0.33	0.63	14.0
+Corr	0.41	0.70	15.0
+Kci+Corr	0.49	0.71	**13.0**

Table 4: Adapting Sea to linear non-Gaussian (Uniform) noise. Lingam run without finetuning; Sea(G) finetuned for distance correlation.

Model	N=10, E=10		N=20, E=20	
	mAP ↑	SHD ↓	mAP ↑	SHD ↓
Dcdi-Dsf	0.34	22.3	0.32	63.0
Lingam*	0.34	7.2	0.30	18.8
Sea (G)	0.26	12.7	0.12	46.6
+lingam	0.52	10.1	0.22	39.7
+dcor	0.44	8.0	0.21	33.1
+ling+dcor	**0.76**	**4.6**	**0.67**	**14.2**

Table 5: Adapting Sea to polynomial, sigmoid non-additive (N=10, E=10). Fci run with Kci test; Sea(F) finetuned for distance correlation.

Model	Polynomial		Sigmoid	
	mAP ↑	SHD ↓	mAP ↑	SHD ↓
Dcdi-Dsf	0.39	9.8	0.81	13.6
Fci*	0.12	10.6	0.53	8.1
Sea (F)	0.22	10.6	0.59	4.8
+kci	0.30	10.6	0.59	5.5
+dcor	0.45	9.6	**0.90**	**2.1**
+kci+dcor	**0.52**	**8.2**	0.86	3.4

Another strategy is to "finetune" the aggregator, either fully or using low-cost methods like LoRA (Hu et al., 2022). Specifically, we keep the same training set and classification objective, while changing the input's featurization, e.g. a different global statistic. Here, we show that finetuning our models for distance correlation (Dcor) is beneficial in both Tables 4 and 5, and the combination of strategies results in the highest performance overall, surpassing the best baseline trained from scratch (Dcdi-Dsf).

On real data from unknown distributions, these two strategies enable the ability to run causal discovery with different assumptions, which may be coupled with unsupervised methods for model selection (Faller et al., 2023). Table 3 illustrates this idea using the Sachs proteomics dataset. Sea can be run directly with a different estimation algorithm (FCI with polynomial kernel "Kci"), or finetuned for around 4-6 hours on 1 A6000 and < 4 GB of GPU memory (correlation "Corr"). In contrast, methods like Avici must simulate new datasets based on each new assumption and re-train/finetune on these data (reportedly around 4 days).

5.3 SEA respects identifiability theory

While the identifiability of specific causal models is not a primary focus of this work, we show that Sea still respects classic identifiability theory. Specifically, while linear Gaussian models are known to be unidentifiable, Table 1 might suggest that both Sea and Dcdi perform quite well on these data – better than would be expected if graphs were only identifiable up to their Markov equivalence classes. This empirical "identifiability" may be the consequence of two findings. Common synthetic data generation schemes tend to result in marginal variances that reflect topological order (Reisach et al., 2021), and in additive noise models, it has been shown that marginal variances that are the "same or weakly monotone increasing in the [topological] ordering" result in uniquely identifiable graphs (Park, 2020). Data standardization can eliminate these artifacts of synthetic data generation. In Table 5.3, we see that after standardizing linear Gaussian data, our model performs no better than randomly selecting a graph from the Markov equivalence class (enumerated

Table 6: Sea respects identifiability theory. Observational setting, *standardized* (-std) $N = 10, E = 10$ linear Gaussian test datasets with > 1 graph in Markov equivalence class (MEC). Top: oracle performance based on true MEC (see left). Bottom: trained Sea approaches oracle performance, while FCI is very noisy.

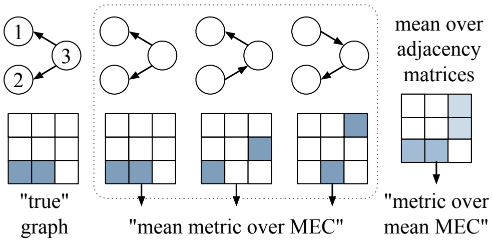

Model	mAP(↑)	AUC(↑)	SHD(↓)	OA(↑)
metric over mean MEC	$0.88 \pm .10$	$0.98 \pm .03$	2.0 ± 1.0	$0.74 \pm .22$
mean metric over MEC	$0.74 \pm .21$	$0.91 \pm .07$	$1.2 \pm .69$	$0.84 \pm .13$
Sea(Fci)-std	$0.83 \pm .16$	$0.97 \pm .04$	3.3 ± 2.3	$0.69 \pm .21$
Sea(Fci)+Corr-std	$0.84 \pm .14$	$0.96 \pm .03$	5.0 ± 4.5	$0.85 \pm .14$
Fci-std	$0.49 \pm .28$	$0.75 \pm .16$	9.3 ± 2.8	$0.49 \pm .29$

Table 7: Sea is generally insensitive to swapping estimation algorithms at *inference* time. Results on $N = 10$ observational setting, all other parameters default. Fci cannot be used with Sea(g) since it outputs edge types beyond those of Gies.

Inference	Sea (Fci)				Sea (Gies)			
estimator	Lin.	NN	Sig.	Poly.	Lin.	NN	Sig.	Poly.
FCI	0.98	0.88	0.83	0.62	—	—	—	—
PC	0.93	0.85	0.86	0.64	0.96	0.89	0.82	0.58
GES	0.94	0.85	0.80	0.60	0.95	0.88	0.81	0.57
GRaSP	0.93	0.85	0.80	0.61	0.95	0.88	0.81	0.57

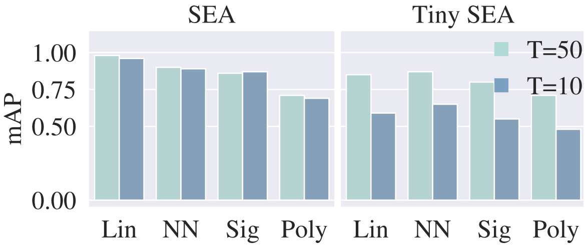

Figure 3: Few-shot learning behavior emerges as training set increases. "Tiny" Sea trained on 1/4 of the data is comparable to the full model on $N = 10$ datasets when given $T = 50$ batches, but is less robust with only $T = 10$.

via `pcalg` (Kalisch et al., 2012)). The classic FCI algorithm is unable to reach this upper bound, suggesting that the amortized inference framework allows us to perform better in finite datasets.

5.4 Ablation studies

In addition to high performance and flexibility, one of the hallmarks of foundation models is their ability to act as few-shot learners when scaling up (Brown et al., 2020). We first confirm that Sea is indeed data-efficient, requiring only around 300-400 examples for performance to converge on datasets of $N = 100$ variables, and outperforms inverse covariance (computed with 500 examples) at only 200 examples (Figure 4A). To probe for how this behavior emerges, we trained a "tiny" version of Sea (Gies) on approximately a quarter of the training data ($N = 10, 20$ datasets, 64.8 million examples). The tiny model performs nearly as well as the original on $N = 10$ datasets when provided $T = 50$ batches, but exhibits much poorer few-shot behavior with only $T = 10$ batches (Figure 3). This demonstrates that Sea is able to ingest large amounts of data, leading to promising few-shot behavior.[5]

We also ablate each parameter of the estimation step to inform best practices. The trade-off between the number and size of batches may be relevant to estimation algorithms that scale poorly with the number of examples, e.g. kernel-based methods (Zhang et al., 2011). When given $T = 100$ batches, Sea reaches reasonable performance at around 250-300 examples per batch (Figure 4B). Figure 4C further illustrates that on the harder Sigmoid datasets, 5 batches of size $b = 500$ are roughly equivalent to 100 batches of size $b = 300$. Finally, increasing the number of variables in each subset has minimal impact (Figure 4D), which is encouraging, as there is no need to incur the exponentially-scaling runtimes associated with larger subsets.

Finally, we analyze the impact of removing marginal estimates or global statistics (Table 8). First, we take a fully pretrained Sea (Gies) and set the corresponding hidden representations to 0. Performance drops more when h^ρ is set to 0, indicating that our *pretrained* aggregator relies more on global statistics, though a sizable gap emerges in both situations. Then, we *re-train* Sea (Gies) on the $N = 10$ datasets, with and without global statistics, so that lack of ρ is in-distribution for the latter model, and the training sets are comparable.

---

[5] Due to computational limitations, we were unable to train larger models, as our existing training set requires several hundred GB in memory, and our file system does not support fast dynamic loading.

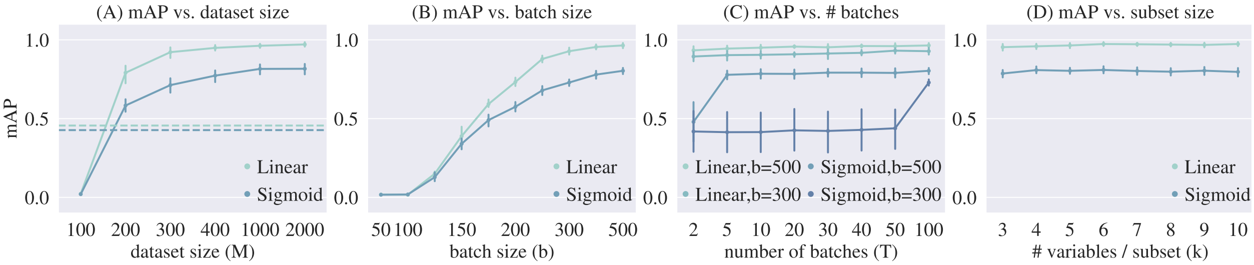

Figure 4: Ablations with Sea (Gies) for estimation parameters on $N = 100, E = 100$. Error bars indicate 95% confidence interval across the 5 datasets of each setting. All parameters are set to the defaults (Section 3.3) unless otherwise noted. (A) Dashed: inverse covariance at $M = 500$. (C) Variance is unusually high for Sigmoid $b = 300$ until $T = 100$, indicating that larger batches result in more stable results.

Table 8: Ablating marginal and global features on Sea (Gies). Top: We set marginal and global representations to 0 (lack of E'/ρ is out-of-distribution) and observe that the pretrained model is more robust to removing E', perhaps since we sample varying T during training. Bottom: Re-train Sea (Gies) on $N = 10$ datasets, with and without global features (lack of ρ is in-distribution). We observe that global features are "worth" $T \approx 40$ estimates of $k = 5$ variables each.

Model	Linear		NN add.		NN.		Sigmoid		Polynomial	
	mAP ↑	SHD ↓	mAP ↑	SHD ↓	mAP ↑	SHD ↓	mAP ↑	SHD ↓	mAP ↑	SHD ↓
Sea (Gies)	0.99±.01	1.2±.7	0.94±.06	2.6±.8	0.91±.07	3.2±.3	0.85±.12	4.0±.5	0.70±.11	5.8±.6
$h^\rho \leftarrow 0$	0.30±.17	29.2±.4	0.27±.18	29.4±.8	0.19±.09	29.0±.0	0.35±.17	27.4±.4	0.31±.15	27.1±.9
$h^E \leftarrow 0$	0.85±.09	6.4±.7	0.82±.11	10.2±.9	0.78±.07	13.2±.2	0.63±.21	10.2±.8	0.55±.19	13.4±.6
$T = 2$	0.20±.04	31.2±.5	0.25±.06	29.2±.4	0.33±.10	27.8±.1	0.19±.07	30.2±.9	0.24±.09	28.1±.9
$T = 10$	0.62±.16	8.0±.8	0.69±.11	9.6±.6	0.66±.13	11.2±.9	0.62±.20	9.2±.6	0.50±.22	8.9±.2
$T = 50$, no ρ	0.63±.13	6.8±.1	0.53±.07	6.2±.9	0.68±.20	6.0±.1	0.58±.15	7.1±.1	0.50±.14	7.1±.5

Here, we see that the "no ρ" version with $T = 50$ estimates is on par with the original architecture with $T = 10$ estimates, so the global statistic is equivalent to ~ 40 estimates. This roughly aligns with the theory that global statistics can expedite the skeleton discovery process (Section 3.4), as the number of estimates required to discover the skeleton of a $N = 10$ graph is approximately $\binom{10}{2} = 45$ (Prop. A.9).

6 Conclusion

Interventional experiments have formed the basis of scientific discovery throughout history, and in recent years, advances in the life sciences have led to datasets of unprecedented scale and resolution (Replogle et al., 2022; Nadig et al., 2024). The goal of these perturbation experiments is to extract causal relationships between biological entities, such as genes or proteins. However, the sheer size, sparsity, and noise level of these data pose significant challenges to existing causal discovery algorithms. Moreover, these real datasets do not fit cleanly into causal frameworks that are designed around fixed sets of data assumptions, either explicit (Spirtes et al., 1995) or implicit (Lorch et al., 2022). In this work, we approached these challenges through a causal discovery "foundation model." Central to this concept were three goals. First, this model should generalize to unseen datasets whose data-generating mechanisms are unknown, and potentially out-of-distribution. Second, it should be easy to steer the model's predictions with inductive biases about the data. Finally, scaling up the model should lead to data-efficiency. We proposed Sea, a framework that yields causal discovery foundation models. Sea was motivated by the idea that classical statistics and discovery algorithms provide powerful descriptors of data that are fast to compute and robust across datasets. Given these statistics, we trained a deep learning model to reproduce faithful causal graphs. Theoretically, we demonstrated that it is possible to produce sound causal graphs from marginal estimates, and that our model has the capacity to do so. Empirically, we implemented two proofs of concept of Sea that perform well across a variety of causal discovery tasks, easily incorporate inductive biases when they are available, and exhibit excellent few-shot behavior when scaled up. In summary, we hope that this work will inspire a new avenue of research into causal discovery algorithms that are applicable to and informed by real applications.

References

Steen A. Andersson, David Madigan, and Michael D. Perlman. A characterization of Markov equivalence classes for acyclic digraphs. *The Annals of Statistics*, 25(2):505 – 541, 1997. doi: 10.1214/aos/1031833662.

Rishi Bommasani, Drew A Hudson, Ehsan Adeli, Russ Altman, Simran Arora, Sydney von Arx, Michael S Bernstein, Jeannette Bohg, Antoine Bosselut, Emma Brunskill, et al. On the opportunities and risks of foundation models. *arXiv preprint arXiv:2108.07258*, 2021.

Andrew P. Bradley. The use of the area under the roc curve in the evaluation of machine learning algorithms. *Pattern Recognition*, 30(7):1145–1159, 1997. ISSN 0031-3203. doi: https://doi.org/10.1016/S0031-3203(96)00142-2.

Philippe Brouillard, Sébastien Lachapelle, Alexandre Lacoste, Simon Lacoste-Julien, and Alexandre Drouin. Differentiable causal discovery from interventional data, 2020.

Tom B. Brown, Benjamin Mann, Nick Ryder, Melanie Subbiah, Jared Kaplan, Prafulla Dhariwal, Arvind Neelakantan, Pranav Shyam, Girish Sastry, Amanda Askell, Sandhini Agarwal, Ariel Herbert-Voss, Gretchen Krueger, Tom Henighan, Rewon Child, Aditya Ramesh, Daniel M. Ziegler, Jeffrey Wu, Clemens Winter, Christopher Hesse, Mark Chen, Eric Sigler, Mateusz Litwin, Scott Gray, Benjamin Chess, Jack Clark, Christopher Berner, Sam McCandlish, Alec Radford, Ilya Sutskever, and Dario Amodei. Language models are few-shot learners, 2020.

Peter Bühlmann, Jonas Peters, and Jan Ernest. CAM: Causal additive models, high-dimensional order search and penalized regression. *The Annals of Statistics*, 42(6):2526 – 2556, 2014. doi: 10.1214/14-AOS1260.

Mathieu Chevalley, Yusuf Roohani, Arash Mehrjou, Jure Leskovec, and Patrick Schwab. CausalBench: A Large-scale Benchmark for Network Inference from Single-cell Perturbation Data. *arXiv preprint arXiv:2210.17283*, 2022.

David Maxwell Chickering. Optimal structure identification with greedy search. *Journal of Machine Learning Research*, 3:507–554, November 2002.

Haotian Cui, Chloe Wang, Hassaan Maan, Kuan Pang, Fengning Luo, Nan Duan, and Bo Wang. scgpt: toward building a foundation model for single-cell multi-omics using generative ai. *Nature Methods*, pp. 1–11, 2024.

Payam Dibaeinia and Saurabh Sinha. Sergio: A single-cell expression simulator guided by gene regulatory networks. *Cell Systems*, 11(3):252–271.e11, 2020. ISSN 2405-4712. doi: https://doi.org/10.1016/j.cels.2020.08.003.

Philipp M. Faller, Leena Chennuru Vankadara, Atalanti A. Mastakouri, Francesco Locatello, Dominik Janzing Karlsruhe Institute of Technology, and Amazon Research Tuebingen. Self-compatibility: Evaluating causal discovery without ground truth. *International Conference on Artificial Intelligence and Statistics*, 2023.

Nir Friedman, Moisés Goldszmidt, and Abraham J. Wyner. Data analysis with bayesian networks: A bootstrap approach. *Proceedings of the Fifteenth Conference on Uncertainty in Artificial Intelligence, UAI'99*, pp. 196–205, 1999.

Tomas Geffner, Javier Antoran, Adam Foster, Wenbo Gong, Chao Ma, Emre Kiciman, Amit Sharma, Angus Lamb, Martin Kukla, Nick Pawlowski, Miltiadis Allamanis, and Cheng Zhang. Deep end-to-end causal inference, 2022.

Clark Glymour, Kun Zhang, and Peter Spirtes. Review of causal discovery methods based on graphical models. *Frontiers in Genetics*, 10, 2019. ISSN 1664-8021. doi: 10.3389/fgene.2019.00524.

Alain Hauser and Peter Bühlmann. Characterization and greedy learning of interventional markov equivalence classes of directed acyclic graphs. *Journal of Machine Learning Research*, 13(79):2409–2464, 2012.

Alain Hauser and Peter Bühlmann. Characterization and greedy learning of interventional markov equivalence classes of directed acyclic graphs. *arXiv*, 2012.

Kurt Hornik, Maxwell Stinchcombe, and Halbert White. Multilayer feedforward networks are universal approximators. *Neural Networks*, 2(5):359–366, 1989. ISSN 0893-6080. doi: https://doi.org/10.1016/0893-6080(89)90020-8.

Edward J Hu, yelong shen, Phillip Wallis, Zeyuan Allen-Zhu, Yuanzhi Li, Shean Wang, Lu Wang, and Weizhu Chen. LoRA: Low-rank adaptation of large language models. In *International Conference on Learning Representations*, 2022. URL `https://openreview.net/forum?id=nZeVKeeFYf9`.

Biwei Huang, Kun Zhang, Mingming Gong, and Clark Glymour. Causal discovery from multiple data sets with non-identical variable sets. *Proceedings of the AAAI Conference on Artificial Intelligence*, 34(06): 10153–10161, Apr. 2020. doi: 10.1609/aaai.v34i06.6575.

Diviyan Kalainathan, Olivier Goudet, and Ritik Dutta. Causal discovery toolbox: Uncovering causal relationships in python. *Journal of Machine Learning Research*, 21(37):1–5, 2020.

Markus Kalisch, Martin Mächler, Diego Colombo, Marloes H Maathuis, and Peter Bühlmann. Causal inference using graphical models with the r package pcalg. *Journal of statistical software*, 47:1–26, 2012.

Nan Rosemary Ke, Silvia Chiappa, Jane Wang, Anirudh Goyal, Jorg Bornschein, Melanie Rey, Theophane Weber, Matthew Botvinic, Michael Mozer, and Danilo Jimenez Rezende. Learning to induce causal structure, 2022.

Sébastien Lachapelle, Philippe Brouillard, Tristan Deleu, and Simon Lacoste-Julien. Gradient-based neural dag learning, 2020.

Wai-Yin Lam, Bryan Andrews, and Joseph Ramsey. Greedy relaxations of the sparsest permutation algorithm. In James Cussens and Kun Zhang (eds.), *Proceedings of the Thirty-Eighth Conference on Uncertainty in Artificial Intelligence*, volume 180 of *Proceedings of Machine Learning Research*, pp. 1052–1062. PMLR, 01–05 Aug 2022.

Olivier Ledoit and Michael Wolf. A well-conditioned estimator for large-dimensional covariance matrices. *Journal of Multivariate Analysis*, 88(2):365–411, 2004. ISSN 0047-259X. doi: https://doi.org/10.1016/S0047-259X(03)00096-4.

Phillip Lippe, Taco Cohen, and Efstratios Gavves. Efficient neural causal discovery without acyclicity constraints. In *International Conference on Learning Representations*, 2022.

Romain Lopez, Jan-Christian Hütter, Jonathan K. Pritchard, and Aviv Regev. Large-scale differentiable causal discovery of factor graphs. In *Advances in Neural Information Processing Systems*, 2022.

Lars Lorch, Scott Sussex, Jonas Rothfuss, Andreas Krause, and Bernhard Schölkopf. Amortized inference for causal structure learning, 2022.

Ilya Loshchilov and Frank Hutter. Decoupled weight decay regularization, 2019.

Francesco Montagna, Max Cairney-Leeming, Dhanya Sridhar, and Francesco Locatello. Demystifying amortized causal discovery with transformers. *arXiv preprint arXiv:2405.16924*, 2024.

Joris M. Mooij, Sara Magliacane, and Tom Claassen. Joint causal inference from multiple contexts. *arXiv*, 2020.

Ajay Nadig, Joseph M. Replogle, Angela N. Pogson, Steven A McCarroll, Jonathan S. Weissman, Elise B. Robinson, and Luke J. O'Connor. Transcriptome-wide characterization of genetic perturbations. *bioRxiv*, 2024. doi: 10.1101/2024.07.03.601903.

Long Ouyang, Jeffrey Wu, Xu Jiang, Diogo Almeida, Carroll Wainwright, Pamela Mishkin, Chong Zhang, Sandhini Agarwal, Katarina Slama, Alex Ray, et al. Training language models to follow instructions with human feedback. *Advances in neural information processing systems*, 35:27730–27744, 2022.

Gunwoong Park. Identifiability of additive noise models using conditional variances. *Journal of Machine Learning Research*, 21(75):1–34, 2020. URL `http://jmlr.org/papers/v21/19-664.html`.

Jorge Pérez, Javier Marinković, and Pablo Barceló. On the turing completeness of modern neural network architectures. In *International Conference on Learning Representations*, 2019.

Alec Radford, Jeffrey Wu, Rewon Child, David Luan, Dario Amodei, Ilya Sutskever, et al. Language models are unsupervised multitask learners. *OpenAI blog*, 1(8):9, 2019.

Alec Radford, Jong Wook Kim, Chris Hallacy, Aditya Ramesh, Gabriel Goh, Sandhini Agarwal, Girish Sastry, Amanda Askell, Pamela Mishkin, Jack Clark, Gretchen Krueger, and Ilya Sutskever. Learning transferable visual models from natural language supervision, 2021.

Roshan M Rao, Jason Liu, Robert Verkuil, Joshua Meier, John Canny, Pieter Abbeel, Tom Sercu, and Alexander Rives. Msa transformer. In Marina Meila and Tong Zhang (eds.), *Proceedings of the 38th International Conference on Machine Learning*, volume 139 of *Proceedings of Machine Learning Research*, pp. 8844–8856. PMLR, 18–24 Jul 2021.

Alexander G. Reisach, Christof Seiler, and Sebastian Weichwald. Beware of the simulated dag! causal discovery benchmarks may be easy to game. *Advances in Neural Information Processing Systems*, 34, 2021.

Patrik Reizinger, Yash Sharma, Matthias Bethge, Bernhard Schölkopf, Ferenc Huszár, and Wieland Brendel. Jacobian-based causal discovery with nonlinear ICA. *Transactions on Machine Learning Research*, 2023. ISSN 2835-8856.

J. M. Replogle, R. A. Saunders, A. N. Pogson, J. A. Hussmann, A. Lenail, A. Guna, L. Mascibroda, E. J. Wagner, K. Adelman, G. Lithwick-Yanai, N. Iremadze, F. Oberstrass, D. Lipson, J. L. Bonnar, M. Jost, T. M. Norman, and J. S. Weissman. Mapping information-rich genotype-phenotype landscapes with genome-scale Perturb-seq. *Cell*, 185(14):2559–2575, Jul 2022.

Laria Reynolds and Kyle McDonell. Prompt programming for large language models: Beyond the few-shot paradigm. In *Extended abstracts of the 2021 CHI conference on human factors in computing systems*, pp. 1–7, 2021.

Yanay Rosen, Maria Brbić, Yusuf Roohani, Kyle Swanson, Ziang Li, and Jure Leskovec. Toward universal cell embeddings: integrating single-cell rna-seq datasets across species with saturn. *Nature Methods*, pp. 1–9, 2024.

Karen Sachs, Omar Perez, Dana Pe'er, Douglas A. Lauffenburger, and Garry P. Nolan. Causal protein-signaling networks derived from multiparameter single-cell data. *Science*, 308(5721):523–529, 2005. doi: 10.1126/science.1105809.

Pedro Sanchez, Xiao Liu, Alison Q. O'Neil, and Sotirios A. Tsaftaris. Diffusion models for causal discovery via topological ordering. In *The Eleventh International Conference on Learning Representations, ICLR 2023, Kigali, Rwanda, May 1-5, 2023*. OpenReview.net, 2023.

Gideon Schwarz. Estimating the Dimension of a Model. *The Annals of Statistics*, 6(2):461 – 464, 1978. doi: 10.1214/aos/1176344136.

Shohei Shimizu, Patrik O. Hoyer, Aapo Hyvarinen, and Antti Kerminen. A linear non-gaussian acyclic model for causal discovery. *Journal of Machine Learning Research*, 7(72):2003–2030, 2006.

Peter Spirtes, Clark Glymour, and Richard Scheines. Causality from probability. In *Conference Proceedings: Advanced Computing for the Social Sciences*, 1990.

Peter Spirtes, Christopher Meek, and Thomas Richardson. Causal inference in the presence of latent variables and selection bias. In *Proceedings of the Eleventh Conference on Uncertainty in Artificial Intelligence*, UAI'95, pp. 499–506, San Francisco, CA, USA, 1995. Morgan Kaufmann Publishers Inc. ISBN 1558603859.

Peter Spirtes, Clark Glymour, and Richard Scheines. *Causation, Prediction, and Search.* MIT Press, 2001. doi: https://doi.org/10.7551/mitpress/1754.001.0001.

G'abor J. Sz'ekely, Maria L. Rizzo, and Nail K. Bakirov. Measuring and testing dependence by correlation of distances. *Annals of Statistics*, 35:2769–2794, 2007.

Robert Tillman, David Danks, and Clark Glymour. Integrating locally learned causal structures with overlapping variables. *Advances in Neural Information Processing Systems*, 21:1665–1672, 01 2008.

Ioannis Tsamardinos, Laura E Brown, and Constantin F Aliferis. The max-min hill-climbing bayesian network structure learning algorithm. *Machine learning*, 65(1):31–78, 2006.

Ashish Vaswani, Noam Shazeer, Niki Parmar, Jakob Uszkoreit, Llion Jones, Aidan N Gomez, Ł ukasz Kaiser, and Illia Polosukhin. Attention is all you need. In I. Guyon, U. Von Luxburg, S. Bengio, H. Wallach, R. Fergus, S. Vishwanathan, and R. Garnett (eds.), *Advances in Neural Information Processing Systems*, volume 30. Curran Associates, Inc., 2017.

Tom S. Verma and Judea Pearl. On the equivalence of causal models. In *Proceedings of the Sixth Conference on Uncertainty in Artificial Intelligence*, 1990.

Yuhao Wang, Liam Solus, Karren Yang, and Caroline Uhler. Permutation-based causal inference algorithms with interventions. In I. Guyon, U. Von Luxburg, S. Bengio, H. Wallach, R. Fergus, S. Vishwanathan, and R. Garnett (eds.), *Advances in Neural Information Processing Systems*, volume 30. Curran Associates, Inc., 2017.

Chulhee Yun, Srinadh Bhojanapalli, Ankit Singh Rawat, Sashank J. Reddi, and Sanjiv Kumar. Are transformers universal approximators of sequence-to-sequence functions? *CoRR*, abs/1912.10077, 2019.

Kun Zhang, J. Peters, Dominik Janzing, and Bernhard Scholkopf. Kernel-based conditional independence test and application in causal discovery. *Conference on Uncertainty in Artificial Intelligence*, 2011.

Xun Zheng, Bryon Aragam, Pradeep Ravikumar, and Eric P. Xing. Dags with no tears: Continuous optimization for structure learning, 2018.

Yujia Zheng, Biwei Huang, Wei Chen, Joseph Ramsey, Mingming Gong, Ruichu Cai, Shohei Shimizu, Peter Spirtes, and Kun Zhang. Causal-learn: Causal discovery in python. *arXiv preprint arXiv:2307.16405*, 2023.

A Proofs and derivations

Our theoretical contributions focus on two primary directions.

1. We formalize the notion of marginal estimates used in this paper, and prove that given sufficient marginal estimates, it is possible to recover a pattern faithful to the global causal graph. We provide lower bounds on the number of marginal estimates required for such a task, and motivate global statistics as an efficient means to reduce this bound.
2. We show that our proposed axial attention has the capacity to recapitulate the reasoning required for marginal estimate resolution. We provide realistic, finite bounds on the width and depth required for this task.

Before these formal discussions, we start with a toy example to provide intuition regarding marginal estimates and constraint-based causal discovery algorithms.

A.1 Toy example: Resolving marginal graphs

Consider the Y-shaped graph with four nodes in Figure 5. Suppose we run the PC algorithm on all subsets of three nodes, and we would like to recover the result of the PC algorithm on the full graph. We illustrate how one might resolve the marginal graph estimates. The PC algorithm consists of the following steps (Spirtes et al., 2001).

1. Start from the fully connected, undirected graph on N nodes.
2. Remove all edges (i,j) where $X_i \perp\!\!\!\perp X_j$.
3. For each edge (i,j) and subsets $S \subseteq [N] \setminus \{i,j\}$ of increasing size $n = 1,2,\ldots,d$, where d is the maximum degree in G, and all $k \in S$ are connected to either i or j: if $X_i \perp\!\!\!\perp X_j \mid S$, remove edge (i,j).
4. For each triplet (i,j,k), such that only edges (i,k) and (j,k) remain, if k was not in the set S that eliminated edge (i,j), then orient the "v-structure" as $i \to k \leftarrow j$.
5. (Orientation propagation) If $i \to j$, edge (j,k) remains, and edge (i,k) has been removed, orient $j \to k$. If there is a directed path $i \rightsquigarrow j$ and an undirected edge (i,j), then orient $i \to j$.

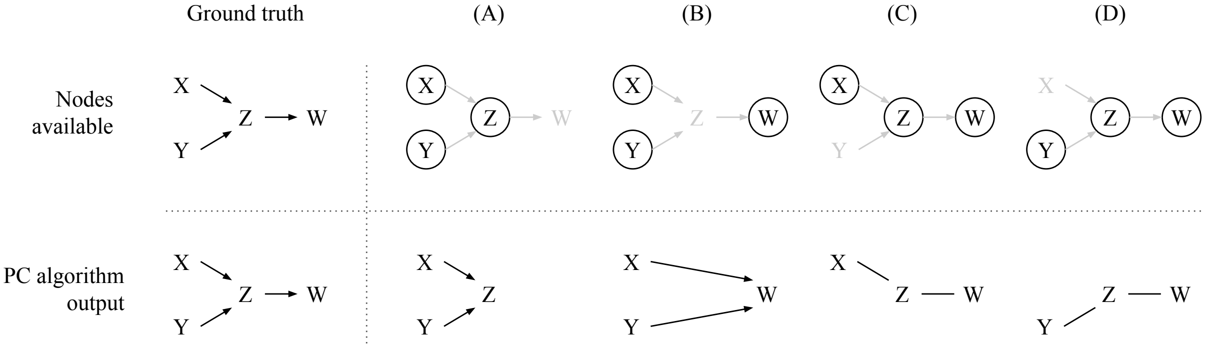

Figure 5: Resolving marginal graphs. Subsets of nodes revealed to the PC algorithm (circled in row 1) and its outputs (row 2).

In each of the four cases, the PC algorithm estimates the respective graphs as follows.

- (A) We remove edge (X,Y) via (2) and orient the v-structure.
- (B) We remove edge (X,Y) via (2) and orient the v-structure.
- (C) We remove edge (X,W) via (3) by conditioning on Z. There are no v-structures, so the edges remain undirected.
- (D) We remove edge (Y,W) via (3) by conditioning on Z. There are no v-structures, so the edges remain undirected.

The outputs (A-D) admit the full PC algorithm output as the only consistent graph on four nodes.

- X and Y are unconditionally independent, so no subset will reveal an edge between (X, Y).
- There are no edges between (X, W) and (Y, W). Otherwise, (C) and (D) would yield the undirected triangle.
- X, Y, Z must be oriented as $X \rightarrow Z \leftarrow Y$. Paths $X \rightarrow Z \rightarrow Y$ and $X \leftarrow Z \leftarrow Y$ would induce an (X, Y) edge in (B). Reversing orientations $X \leftarrow Z \rightarrow Y$ would contradict (A).
- (Y, Z) must be oriented as $Y \rightarrow Z$. Otherwise, (A) would remain unoriented.

A.2 Resolving marginal estimates into global graphs

Classical results have characterized the Markov equivalency class of directed acyclic graphs. Two graphs are observationally equivalent if they have the same skeleton and v-structures (Verma & Pearl, 1990). Thus, a pattern P is *faithful* to a graph G if and only if they share the same skeletons and v-structures (Spirtes et al., 1990).

Definition A.1. Let $G = (V, E)$ be a directed acyclic graph. A *pattern* P is a set of directed and undirected edges over V.

Definition A.2 (Theorem 3.4 from Spirtes et al. (2001))**.** If pattern P is *faithful* to some directed acyclic graph, then P is faithful to G if and only if

1. for all vertices X, Y of G, X and Y are adjacent if and only if X and Y are dependent conditional on every set of vertices of G that does not include X or Y; and
2. for all vertices X, Y, Z, such that X is adjacent to Y and Y is adjacent to Z and X and Z are not adjacent, $X \rightarrow Y \leftarrow Z$ is a subgraph of G if and only if X, Z are dependent conditional on every set containing Y but not X or Z.

Given data faithful to G, a number of classical constraint-based algorithms produce patterns that are faithful to G. We denote this set of algorithms as $\mathcal{F}$.

Theorem A.3 (Theorem 5.1 from Spirtes et al. (2001))**.** *If the input to the PC, SGS, PC-1, PC-2, PC*, or IG algorithms faithful to directed acyclic graph G, the output is a pattern that represents the faithful indistinguishability class of G.*

The algorithms in $\mathcal{F}$ are sound and complete *if* there are no unobserved confounders.

Let P_V be a probability distribution that is Markov, minimal, and faithful to G. Let $D \in \mathbb{R}^{M \times N} \sim P_V$ be a dataset of M observations over all $N = |V|$ nodes.

Consider a subset $S \subseteq V$. Let $D[S]$ denote the subset of D over S,

$$D[S] = \{x_{i,v} : v \in S\}_{i=1}^{N}, \tag{13}$$

and let $G[S]$ denote the subgraph of G induced by S

$$G[S] = (S, \{(i,j) : i, j \in S, (i,j) \in E\}. \tag{14}$$

If we apply any $f \in \mathcal{F}$ to $D[S]$, the results are *not* necessarily faithful to $G[S]$, as now there may be latent confounders in $V \setminus S$ (by construction). We introduce the term *marginal estimate* to denote the resultant pattern that, while not faithful to $G[S]$, is still informative.

Definition A.4 (Marginal estimate)**.** A pattern E' is a *marginal estimate* of $G[S]$ if and only if

1. for all vertices X, Y of S, X and Y are adjacent if and only if X and Y are dependent conditional on every set of vertices of S that does not include X or Y; and
2. for all vertices X, Y, Z, such that X is adjacent to Y and Y is adjacent to Z and X and Z are not adjacent, $X \rightarrow Y \leftarrow Z$ is a subgraph of S if and only if X, Z are dependent conditional on every set containing Y but not X or Z.

Algorithm 1 Resolve marginal estimates of $f \in \mathcal{F}$

```
1: Input: Data $\mathcal{D}_G$ faithful to $G$
2: Initialize $E' \leftarrow K_N$ as the complete undirected graph on $N$ nodes.
3: for $S \in \mathcal{S}_{d+2}$ do
4:     Compute $E'_S = f(\mathcal{D}_{G[S]})$
5:     for $(i, j) \notin E'_S$ do
6:         Remove $(i, j)$ from $E'$
7:     end for
8: end for
9: for $E'_S \in \{E'_S\}_{\mathcal{S}_{d+2}}$ do
10:     for v-structure $i \to j \leftarrow k$ in $E'_S$ do
11:         if $\{i, j\}, \{j, k\} \in E'$ and $\{i, k\} \notin E'$ then
12:             Assign orientation $i \to j \leftarrow k$ in $E'$
13:         end if
14:     end for
15: end for
16: Propagate orientations in $E'$ (optional).
```

Proposition A.5. *Let $G = (V, E)$ be a directed acyclic graph with maximum degree d. For $S \subseteq V$, let E'_S denote the marginal estimate over S. Let $\mathcal{S}_d$ denote the superset that contains all subsets $S \subseteq V$ of size at most d. Algorithm 1 maps $\{E'_S\}_{S \in \mathcal{S}_{d+2}}$ to a pattern E' faithful to G.*

On a high level, lines 3-8 recover the undirected "skeleton" graph of E^*, lines 9-15 recover the v-structures, and line 16 references step 5 in Section A.1.

Remark A.6. In the PC algorithm (Spirtes et al. (2001), A.1), its derivatives, and Algorithm 1, there is no need to consider separating sets with cardinality greater than maximum degree d, since the maximum number of independence tests required to separate any node from the rest of the graph is equal to number of its parents plus its children (due to the Markov assumption).

Lemma A.7. *The undirected skeleton of E^* is equivalent to the undirected skeleton of E'*

$$C^* := \{\{i, j\} \mid (i, j) \in E^* \text{ or } (j, i) \in E^*\} = \{\{i, j\} \mid (i, j) \in E' \text{ or } (j, i) \in E'\} := C'. \tag{15}$$

That is, $\{i, j\} \in C^* \iff \{i, j\} \in C'$.

Proof. It is equivalent to show that $\{i, j\} \notin C^* \iff \{i, j\} \notin C'$

$\Rightarrow$ If $\{i, j\} \notin C*$, then there must exist a separating set S in G of at most size d such that $i \perp\!\!\!\perp j \mid S$. Then $S \cup \{i, j\}$ is a set of at most size $d + 2$, where $\{i, j\} \notin C'_{S \cup \{i,j\}}$. Thus, $\{i, j\}$ would have been removed from C' in line 6 of Algorithm 1.

$\Leftarrow$ If $\{i, j\} \notin C'$, let S be a separating set in $\mathcal{S}_{d+2}$ such that $\{i, j\} \notin C'_{S \cup \{i,j\}}$ and $i \perp\!\!\!\perp j \mid S$. S is also a separating set in G, and conditioning on S removes $\{i, j\}$ from C^*. □

Lemma A.8. *A v-structure $i \to j \leftarrow k$ exists in E^* if and only if there exists the same v-structure in E'.*

Proof. The PCI algorithm orients v-structures $i \to j \leftarrow k$ in E^* if there is an edge between $\{i, j\}$ and $\{j, k\}$ but not $\{i, k\}$; and if j was not in the conditioning set that removed $\{i, k\}$. Algorithm 1 orients v-structures $i \to j \leftarrow k$ in E' if they are oriented as such in any E'_S; and if $\{i, j\}, \{j, k\} \in E', \{i, k\} \notin E'$

$\Rightarrow$ Suppose for contradiction that $i \to j \leftarrow k$ is oriented as a v-structure in E^*, but not in E'. There are two cases.

1. No E'_S contains the undirected path $i - j - k$. If either $i - j$ or $j - k$ are missing from any E'_S, then E^* would not contain (i, j) or (k, j). Otherwise, if all S contain $\{i, k\}$, then E^* would not be missing $\{i, k\}$ (Lemma A.7).

2. In every E'_S that contains $i - j - k$, j is in the conditioning set that removed $\{i, k\}$, i.e. $i \perp\!\!\!\perp k \mid S, S \ni j$. This would violate the faithfulness property, as j is neither a parent of i or k in E^*, and the outputs of the PC algorithm are faithful to the equivalence class of G (Theorem 5.1 Spirtes et al. (2001)).

$\Leftarrow$ Suppose for contradiction that $i \rightarrow j \leftarrow k$ is oriented as a v-structure in E', but not in E^*. By Lemma A.7, the path $i - j - k$ must exist in E^*. There are two cases.

1. If $i \rightarrow j \rightarrow k$ or $i \leftarrow j \leftarrow k$, then j must be in the conditioning set that removes $\{i, k\}$, so no E'_S containing $\{i, j, k\}$ would orient them as v-structures.
2. If j is the root of a fork $i \leftarrow j \rightarrow k$, then as the parent of both i and k, j must be in the conditioning set that removes $\{i, k\}$, so no E'_S containing $\{i, j, k\}$ would orient them as v-structures.

Therefore, all v-structures in E' are also v-structures in E^*. ☐

Proof of Proposition A.5. Given data that is faithful to G, Algorithm 1 produces a pattern E' with the same connectivity and v-structures as E^*. Any additional orientations in both patterns are propagated using identical, deterministic procedures, so $E' = E^*$. ☐

This proof presents a deterministic but inefficient algorithm for resolving marginal subgraph estimates. In reality, it is possible to recover the undirected skeleton and the v-structures of G without checking all subsets $S \in \mathcal{S}_{d+2}$.

Proposition A.9 (Skeleton bounds)**.** *Let $G = (V, E)$ be a directed acyclic graph with maximum degree d. It takes $O(N^2)$ marginal estimates over subsets of size $d + 2$ to recover the undirected skeleton of G.*

Proof. Following Lemma A.7, an edge (i, j) is not present in C if it is not present in any of the size $d + 2$ estimates. Therefore, every pair of nodes $\{i, j\}$ requires only a single estimate of size $d + 2$, so it is possible to recover C in $\binom{N}{2}$ estimates. ☐

Proposition A.10 (V-structures bounds)**.** *Let $G = (V, E)$ be a directed acyclic graph with maximum degree d and ν v-structures. It is possible to identify all v-structures in $O(\nu)$ estimates over subsets of at most size $d + 2$.*

Proof. Each v-structure $i \rightarrow j \leftarrow k$ falls under two cases.

1. $i \perp\!\!\!\perp k$ unconditionally. Then an estimate over $\{i, j, k\}$ will identify the v-structure.
2. $i \perp\!\!\!\perp k \mid S$, where $j \notin S \subset V$. Then an estimate over $S \cup \{i, j, k\}$ will identify the v-structure. Note that $|S| \leq d + 2$ since the degree of i is at least $|S| + 1$.

Therefore, each v-structure only requires one estimate, and it is possible to identify all v-structures in $O(\nu)$ estimates. ☐

There are three takeaways from this section.

1. If we exhaustively run a constraint-based algorithm on all subsets of size $d + 2$, it is trivial to recover the estimate of the full graph. However, this is no more efficient than running the causal discovery algorithm on the full graph.
2. In theory, it is possible to recover the undirected graph in $O(N^2)$ estimates, and the v-structures in $O(\nu)$ estimates. However, we may not know the appropriate subsets ahead of time.
3. In practice, if we have a surrogate for connectivity, such as the global statistics used in SEA, then we can vastly reduce the number of estimates used to eliminate edges from consideration, and more effectively focus on sampling subsets for orientation determination.

A.3 Computational power of the axial attention model

Existing literature on the universality and computational power of vanilla Transformers (Yun et al., 2019; Pérez et al., 2019) rely on generous assumptions regarding depth or precision. Here, we show that our axial attention-based model can implement the specific reasoning required to resolve marginal estimates under realistic conditions. In particular, we show that three blocks can recover the skeleton and v-structures in $O(N)$ width, and additional blocks have the capacity to propagate orientations. We first formalize the notion of a neural network architecture's capacity to "implement" an algorithm. Then we prove Theorem 3.1 by construction.

Definition A.11. Let f be a map from finite sets Q to F, and let ϕ be a map from finite sets Q_Φ to F_Φ. We say ϕ *implements* f if there exists injection $g_{\text{in}} : Q \to Q_\Phi$ and surjection $g_{\text{out}} : F_\Phi \to F$ such that

$$\forall q \in Q, g_{\text{out}}(\phi(g_{\text{in}}(q))) = f(q). \tag{16}$$

Definition A.12. Let Q, F, Q_Φ, F_Φ be finite sets. Let f be a map from Q to F, and let Φ be a finite set of maps $\{\phi : Q_\Phi \to F_\Phi\}$. We say Φ has the *capacity* to implement f if and only if there exists at least one element $\phi \in \Phi$ that implements f.

Theorem 3.1. *Let $G = (V, E)$ be a directed acyclic graph with maximum degree d. For $S \subseteq V$, let E'_S denote the marginal estimate over S. Let $\mathcal{S}_d$ denote the superset that contains all subsets $S \subseteq V$ of size at most d. Given $\{E'_S\}_{S \in \mathcal{S}_{d+2}}$, a stack of L axial attention blocks has the capacity to recover G's skeleton and v-structures in $O(N)$ width, and propagate orientations on paths of $O(L)$ length.*

Proof. We consider axial attention blocks with dot-product attention and omit layer normalization from our analysis, as is common in the Transformer universality literature Yun et al. (2019). Our inputs $X \in \mathbb{R}^{d \times R \times C}$ consist of d-dimension embeddings over R rows and C columns. Since our axial attention only operates over one dimension at a time, we use $X_{\cdot,c}$ to denote a 1D sequence of length R, given a fixed column c, and $X_{r,\cdot}$ to denote a 1D sequence of length C, given a fixed row r. A single axial attention layer (with one head) consists of two attention layers and a feedforward network,

$$\begin{aligned}
\text{Attn}_{\text{row}}(X_{\cdot,c}) &= X_{\cdot,c} + W_O W_V X_{\cdot,c} \cdot \sigma\left[(W_K X_{\cdot,c})^T W_Q X_{\cdot,c}\right], && (17)\\
X &\leftarrow \text{Attn}_{\text{row}}(X) \\
\text{Attn}_{\text{col}}(X_{r,\cdot}) &= X_{r,\cdot} + W_O W_V X_{r,\cdot} \cdot \sigma\left[(W_K X_{r,\cdot})^T W_Q X_{r,\cdot}\right], && (18)\\
X &\leftarrow \text{Attn}_{\text{col}}(X) \\
\text{FFN}(X) &= X + W_2 \cdot \text{ReLU}(W_1 \cdot X + b_1 \mathbf{1}_L^T) + b_2 \mathbf{1}_L^T, && (19)
\end{aligned}$$

where $W_O \in \mathbb{R}^{d \times d}, W_V, W_K, W_Q \in \mathbb{R}^{d \times d}, W_2 \in \mathbb{R}^{d \times m}, W_1 \in \mathbb{R}^{m \times d}, b_2 \in \mathbb{R}^d, b_1 \in \mathbb{R}^m$, and m is the hidden layer size of the feedforward network. For concision, we have omitted the r and c subscripts on the Ws, but the row and column attentions use different parameters. Any row or column attention can take on the identity mapping by setting W_O, W_V, W_K, W_Q to $d \times d$ matrices of zeros.

A single axial attention *block* consists of two axial attention layers ϕ_E and ϕ_ρ, connected via messages (Section 3.3)

$$\begin{aligned}
h^{E,\ell} &= \phi_{E,\ell}(h^{E,\ell-1}) \\
h^{\rho,\ell-1} &\leftarrow W_{\rho,\ell}\left[h^{\rho,\ell-1}, m^{E\to\rho,\ell}\right] \\
h^{\rho,\ell} &= \phi_{\rho,\ell}(h^{\rho,\ell-1}) \\
h^{E,\ell} &\leftarrow h^{E,\ell} + m^{\rho\to E,\ell}
\end{aligned}$$

where h^ℓ denote the hidden representations of E and ρ at layer ℓ, and the outputs of the axial attention block are $h^{\rho,\ell}, h^{E,\ell}$.

We construct a stack of $L \geq 3$ axial attention blocks that implement Algorithm 1.

Model inputs Consider edge estimate $E'_{i,j} \in \mathcal{E}$ in a graph of size N. Let e_i, e_j denote the endpoints of (i, j). Outputs of the PC algorithm can be expressed by three endpoints: $\{\varnothing, \bullet, \blacktriangleright\}$. A directed edge from $i \to j$ has endpoints $(\bullet, \blacktriangleright)$, the reversed edge $i \leftarrow j$ has endpoints $(\blacktriangleright, \bullet)$, an undirected edge has endpoints $(\bullet, \bullet)$, and the lack of any edge between i, j has endpoints $(\varnothing, \varnothing)$.

Let one-hot$_N(i)$ denote the N-dimensional one-hot column vector where element i is 1. We define the embedding of (i, j) as a $d = 2N + 6$ dimensional vector,

$$g_{\text{in}}(E_{t,(i,j)}) = h^{E,0}_{(i,j)} = \left[\begin{array}{c} \text{one-hot}_3(e_i) \\ \hline \text{one-hot}_3(e_j) \\ \hline \text{one-hot}_N(i) \\ \hline \text{one-hot}_N(j) \end{array}\right]. \tag{20}$$

To recover graph structures from h^E, we simply read off the indices of non-zero entries (g_{out}). We can set $h^{\rho,0}$ to any $\mathbb{R}^{d\times N\times N}$ matrix, as we do not consider its values in this analysis and discard it during the first step.

Claim A.13. *(Consistency) The outputs of each step*

1. *are consistent with (20), and*
2. *are equivariant to the ordering of nodes in edges.*

For example, if (i, j) is oriented as $(\blacktriangleright, \bullet)$, then we expect (j, i) to be oriented $(\bullet, \blacktriangleright)$.

Step 1: Undirected skeleton We use the first axial attention block to recover the undirected skeleton C'. We set all attentions to the identity, set $W_{\rho,1} \in \mathbb{R}^{2d\times d}$ to a $d \times d$ zeros matrix, stacked on top of a $d \times d$ identity matrix (discard ρ), and set FFN$_E$ to the identity (inputs are positive). This yields

$$h^{\rho,0}_{i,j} = m^{E\to\rho,1}_{i,j} = \left[\begin{array}{c} P_{e_i}(\varnothing) \\ P_{e_i}(\bullet) \\ P_{e_i}(\blacktriangleright) \\ \hline \vdots \\ \hline \text{one-hot}_N(i) \\ \hline \text{one-hot}_N(j) \end{array}\right], \tag{21}$$

where $P_{e_i}(\cdot)$ is the frequency that endpoint $e_i = \cdot$ within the subsets sampled. FFNs with 1 hidden layer are universal approximators of continuous functions (Hornik et al., 1989), so we use FFN$_\rho$ to map

$$\text{FFN}_\rho(X_{i,u,v}) = \begin{cases} 0 & i \le 6 \\ 0 & i > 6, X_{1,u,v} = 0 \\ -X_{i,u,v} & \text{otherwise,} \end{cases} \tag{22}$$

where $i \in [2N + 6]$ indexes into the feature dimension, and u, v index into the rows and columns. This allows us to remove edges not present in C' from consideration:

$$\begin{aligned} m^{\rho\to E,1} &= h^{\rho,1} \\ h^{E,1}_{i,j} \leftarrow h^{E,1}_{i,j} + m^{\rho\to E,1}_{i,j} &= \begin{cases} 0 & (i,j) \notin C' \\ h^{E,0}_{i,j} & \text{otherwise.} \end{cases} \end{aligned} \tag{23}$$

This yields $(i, j) \in C'$ if and only if $h^{\rho,1}_{i,j} \neq \mathbf{0}$. We satisfy A.13 since our inputs are valid PC algorithm outputs for which $P_{e_i}(\varnothing) = P_{e_j}(\varnothing)$.

Step 2: V-structures The second and third axial attention blocks recover v-structures. We run the same procedure twice, once to capture v-structures that point towards the first node in an ordered pair, and one to capture v-structures that point towards the latter node.

We start with the first row attention over edge estimates, given a fixed subset t. We set the key and query attention matrices

$$W_K = k \cdot \begin{bmatrix} 0 & 0 & 1 & & & & & \\ & & & 0 & 1 & 0 & & \\ & \vdots & & & & & & \\ & & & & & & I_N & \\ & & & & & & & -I_N \end{bmatrix} \qquad W_Q = k \cdot \begin{bmatrix} 0 & 0 & 1 & & & & & \\ & & & 0 & 1 & 0 & & \\ & \vdots & & & & & & \\ & & & & & & I_N & \\ & & & & & & & I_N \end{bmatrix} \tag{24}$$

where k is a large constant, I_N denotes the size N identity matrix, and all unmarked entries are 0s.

Recall that a v-structure is a pair of directed edges that share a target node. We claim that two edges $(i,j),(u,v)$ form a v-structure in E', pointing towards $i=u$, if this inner product takes on the maximum value

$$\left\langle (W_K h^{E,1})_{i,j}, (W_Q h^{E,1})_{u,v} \right\rangle = 3. \tag{25}$$

Suppose both edges (i,j) and (u,v) still remain in C'. There are two components to consider.

1. If $i=u$, then their shared node contributes $+1$ to the inner product (prior to scaling by k). If $j=v$, then the inner product accrues -1.
2. Nodes that do not share the same endpoint contribute 0 to the inner product. Of edges that share one node, only endpoints that match ▶ at the starting node, or ● at the ending node contribute $+1$ to the inner product each. We provide some examples below.

(e_i, e_j)	(e_u, e_v)	contribution	note
(▶, ●)	(●, ▶)	0	no shared node
(●, ▶)	(●, ▶)	0	wrong endpoints
(●, ●)	(●, ●)	1	one correct endpoint
(▶, ●)	(▶, ●)	2	v-structure

All edges with endpoints $\varnothing$ were "removed" in step 1, resulting in an inner product of zero, since their node embeddings were set to zero. We set k to some large constant (empirically, $k^2 = 1000$ is more than enough) to ensure that after softmax scaling, $\sigma_{e,e'} > 0$ only if e, e' form a v-structure.

Given ordered pair $e=(i,j)$, let $V_i \subset V$ denote the set of nodes that form a v-structure with e with shared node i. Note that V_i excludes j itself, since setting of W_K, W_Q exclude edges that share both nodes. We set W_V to the identity, and we multiply by attention weights σ to obtain

$$(W_V h^{E,1}\sigma)_{e=(i,j)} = \left[\begin{array}{c} \vdots \\ \hline \text{one-hot}_N(i) \\ \hline \alpha_j \cdot \text{binary}_N(V_j) \end{array}\right] \tag{26}$$

where $\text{binary}_N(S)$ denotes the N-dimensional binary vector with ones at elements in S, and the scaling factor

$$\alpha_j = (1/\|V_j\|) \cdot \mathbb{1}\{\|V_j\| > 0\} \in [0,1] \tag{27}$$

results from softmax normalization. We set

$$W_O = \begin{bmatrix} \mathbf{0}_{N+6} & \\ & 0.5 \cdot I_N \end{bmatrix} \tag{28}$$

to preserve the original endpoint values, and to distinguish between the edge's own node identity and newly recognized v-structures. To summarize, the output of this row attention layer is

$$\text{Attn}_{\text{row}}(X_{\cdot,c}) = X_{\cdot,c} + W_O W_V X_{\cdot,c} \cdot \sigma,$$

which is equal to its input $h^{E,1}$ plus additional positive values $\in (0, 0.5)$ in the last N positions that indicate the presence of v-structures that exist in the overall E'.

Our final step is to "copy" newly assigned edge directions into all the edges. We set the ϕ_E column attention, FFN_E and the ϕ_ρ attentions to the identity mapping. We also set $W_{\rho,2}$ to a $d \times d$ zeros matrix, stacked on top of a $d \times d$ identity matrix. This passes the output of the ϕ_E row attention, aggregated over subsets, directly to $\text{FFN}_{\phi,2}$.

For endpoint dimensions $\mathbf{e} = [6]$, we let $\text{FFN}_{\phi,2}$ implement

$$\text{FFN}_{\rho,2}(X_{\mathbf{e},u,v}) = \begin{cases} [0,0,1,0,1,0]^T - X_{\mathbf{e},u,v} & 0 < \sum_{i>N+6} X_{i,u,v} < 0.5 \\ 0 & \text{otherwise.} \end{cases} \tag{29}$$

Subtracting $X_{\mathbf{e},u,v}$ "erases" the original endpoints and replaces them with $(\blacktriangleright, \bullet)$ after the update

$$h^{E,1}_{i,j} \leftarrow h^{E,1}_{i,j} + m^{\rho \to E,1}_{i,j}.$$

The overall operation translates to checking whether *any* v-structure points towards i, and if so, assigning edge directions accordingly. For dimensions $i > 6$,

$$\text{FFN}_{\rho,2}(X_{i,u,v}) = \begin{cases} -X_{i,u,v} & X_{i,u,v} \leq 0.5 \\ 0 & \text{otherwise,} \end{cases} \tag{30}$$

effectively erasing the stored v-structures from the representation and remaining consistent to (20).

At this point, we have copied all v-structures once. However, our orientations are not necessarily symmetric. For example, given v-structure $i \to j \leftarrow k$, our model orients edges (j, i) and (j, k), but not (i, j) or (k, j).

The simplest way to symmetrize these edges (for the writer and the reader) is to run another axial attention block, in which we focus on v-structures that point towards the second node of a pair. The only changes are as follows.

- For W_K and W_Q, we swap columns 1-3 with 4-6, and columns 7 to $N + 6$ with the last N columns.
- $(h^{E,2}\sigma)_{i,j}$ sees the third and fourth blocks swapped.
- W_O swaps the $N \times N$ blocks that correspond to i and j's node embeddings.
- $\text{FFN}_{\rho,3}$ sets the endpoint embedding to $[0, 1, 0, 0, 0, 1]^T - X_{\mathbf{e},u,v}$ if $i = 7, ..., N + 6$ sum to a value between 0 and 0.5.

The result is $h^{E,3}$ with all v-structures oriented symmetrically, satisfying A.13.

Step 3: Orientation propagation To propagate orientations, we would like to identify cases $(i, j), (i, k) \in E', (j, k) \notin E'$ with shared node i and corresponding endpoints $(\blacktriangleright, \bullet), (\bullet, \bullet)$. We use ϕ_E to identify triangles, and ϕ_ρ to identify edges $(i, j), (i, k) \in E'$ with the desired endpoints, while ignoring triangles.

Marginal layer The row attention in ϕ_E fixes a subset t and varies the edge (i, j).

Given edge (i, j), we want to extract all (i, k) that share node i. We set the key and query attention matrices to

$$W_K, W_Q = k \cdot \begin{bmatrix} 0 & 1 & 1 & 0 & 1 & 1 & & \\ \vdots & & & & & & & \\ & & & & & & I_N & \\ & & & & & & & \pm I_N \end{bmatrix}. \tag{31}$$

We set W_V to the identity to obtain

$$(W_V h^E \sigma)_{e=(i,k)} = \left[\begin{array}{c} \vdots \\ \hline \vdots \\ \hline \text{one-hot}_N(i) \\ \hline \alpha_k \cdot \text{binary}_N(V_k) \end{array} \right], \tag{32}$$

where V_k is the set of nodes k that share any edge with i. To distinguish between k and V_k, we again set W_o to the same as in (28). Finally, we set FFN_E to the identity and pass h^E directly to ϕ_ρ. To summarize, we have h^E equal to its input, with values $\in (0, 0.5)$ in the last N locations indicating 1-hop neighbors of each edge.

Global layer Now we would like to identify cases $(i,k),(j,k)$ with corresponding endpoints $(\bullet, \blacktriangleright), (\bullet, \bullet)$. We set the key and query attention matrices

$$W_K = k \cdot \begin{bmatrix} 0 & 0 & 1 & & \\ \vdots & & & & \\ & & & I_N & \\ & & & & I_N \end{bmatrix} \qquad W_Q = k \cdot \begin{bmatrix} 0 & 1 & -1 & 0 & 1 & -1 & & \\ \vdots & & & & & & & \\ & & & & & & I_N & \\ & & & & & & & -I_N \end{bmatrix}. \tag{33}$$

The key allows us to check that endpoint i is directed, and the query allows us to check that (i,k) exists in C', and does not already point elsewhere. After softmax normalization, for sufficiently large k, we obtain $\sigma_{(i,j),(i,k)} > 0$ if and only if (i,k) should be oriented $(\bullet, \blacktriangleright)$, and the inner product attains the maximum possible value

$$\langle (W_K h^\rho)_{i,j}, (W_Q h^\rho)_{i,k} \rangle = 2. \tag{34}$$

We consider two components.

1. If the endpoints match our desired endpoints, we gain a $+1$ contribution to the inner product.
2. A match between the first nodes contributes $+1$. If the second node shares any overlap (either same edge, or a triangle), then a negative value would be added to the overall inner product.

Therefore, we can only attain the maximal inner product if only one edge is directed, and if there exists no triangle.

We set W_o to the same as in (28), and we add h^ρ to the input of the next ϕ_E. To summarize, we have h^ρ equal to its input, with values $\in (0, 0.5)$ in the last N locations indicating incoming edges.

Orientation assignment Our final step is to assign our new edge orientations. Let the column attention take on the identity mapping. For endpoint dimensions $\mathbf{e} = (4,5,6)$, we let FFN_ρ implement

$$\text{FFN}_\rho(X_{\mathbf{e},u,v}) = \begin{cases} [0,0,1]^T - X_{\mathbf{e},u,v} & 0 < \sum_{i>N+6} X_{i,u,v} < 0.5 \\ 0 & \text{otherwise.} \end{cases} \tag{35}$$

This translates to checking whether any incoming edge points towards v, and if so, assigning the new edge direction accordingly. For dimensions $i > 6$,

$$\text{FFN}_\rho(X_{i,u,v}) = \begin{cases} 0 & X_{i,u,v} \leq 0.5 \\ X_{i,u,v} & \text{otherwise,} \end{cases} \tag{36}$$

effectively erasing the stored assignments from the representation. Thus, we are left with $h^{E,\ell}$ that conforms to the same format as the initial embedding in (20).

To symmetrize these edges, we run another axial attention block, in which we focus on paths that point towards the second node of a pair. The only changes are as follows.

- For ϕ_E layer W_K and W_Q (31), we swap I_N and $\pm I_N$.
- For ϕ_ρ layer W_K and W_Q (33), we swap I_N and $\pm I_N$.
- W_O swaps the $N \times N$ blocks that correspond to i and j's node embeddings.
- For FFN_ρ (35), we let $\mathbf{e} = (1,2,3)$ instead.

The result is h^E with symmetric 1-hop orientation propagation, satisfying A.13. We may repeat this procedure k times to capture k-hop paths.

To summarize, we used axial attention block 1 to recover the undirected skeleton C', blocks 2-3 to identify and copy v-structures in E', and all subsequent $L-3$ layers to propagate orientations on paths up to $\lfloor (L-3)/2 \rfloor$ length. Overall, this particular construction requires $O(N)$ width for $O(L)$ paths.

$\square$

Final remarks Information theoretically, it should be possible to encode the same information in $\log N$ space, and achieve $O(\log N)$ width. For ease of construction, we have allowed for wider networks than optimal. On the other hand, if we increase the width and encode each edge symmetrically, e.g. $(e_i, e_j, e_j, e_i \mid i, j, j, i)$, we can reduce the number of blocks by half, since we no longer need to run each operation twice. However, attention weights scale quadratically, so we opted for an asymmetric construction.

Finally, a strict limitation of our model is that it only considers 1D pairwise interactions. In the graph layer, we cannot compare different edges' estimates at different times in a single step. In the feature layer, we cannot compare (i, j) to (j, i) in a single step either. However, the graph layer does enable us to compare all edges at once (sparsely), and the feature layer looks at a time-collapsed version of the whole graph. Therefore, though we opted for this design for computational efficiency, we have shown that it is able to capture significant graph reasoning.

A.4 Robustness and stability

We discuss the notion of stability informally, in the context of Spirtes et al. (2001). There are two cases in which our framework may receive erroneous inputs: low/noisy data settings, and functionally misspecified situations. We consider our framework's empirical robustness to these cases, in terms of recovering the skeleton and orienting edges.

In the case of noisy data, edges may be erroneously added, removed, or misdirected from marginal estimates E'. Our framework provides two avenues to mitigating such noise.

1. We observe that global statistics can be estimated reliably in low data scenarios. For example, Figure 4 suggests that 250 examples suffice to provide a robust estimate over 100 variables in our synthetic settings. Therefore, even if the marginal estimates are erroneous, the neural network can learn the skeleton from the global statistics.
2. Most classical causal discovery algorithms are not stable with respect to edge orientation assignment. That is, an error in a single edge may propagate throughout the graph. Empirically, we observe that the majority vote of GIES achieves reasonable accuracy even without any training, while FCI suffers in this assessment (Table 10). However both SEA (GIES) and SEA (FCI) achieve high edge accuracy. Therefore, while the underlying algorithms may not be stable with respect to edge orientation, our pretrained aggregator seems to be robust.

It is also possible that our global statistics and marginal estimates make misspecified assumptions regarding the data generating mechanisms. The degree of misspecification can vary case by case, so it is hard to provide any broad guarantees about the performance of our algorithm, in general. However, we can make the following observation.

If two variables are independent, $X_i \perp\!\!\!\perp X_j$, they are independent, e.g. under linear Gaussian assumptions. If X_i, X_j exhibit more complex functional dependencies, they may be erroneously deemed independent. Therefore, any systematic errors are necessarily one-sided, and the model can learn to recover the connectivity based on global statistics.

B Experimental details

B.1 Synthetic data generation

Synthetic datasets were generated using code from DCDI (Brouillard et al., 2020), which extended the Causal Discovery Toolkit data generators to interventional data (Kalainathan et al., 2020).

We considered the following causal mechanisms. Let y be the node in question, let X be its parents, let E be an independent noise variable (details below), and let W be randomly initialized weight matrices.

- Linear: $y = XW + E$.
- Polynomial: $y = W_0 + XW_1 + X^2W_2 + \times E$

- Sigmoid: $y = \sum_{i=1}^{d} W_i \cdot \text{sigmoid}(X_i) + \times E$
- Randomly initialized neural network (NN): $y = \text{Tanh}((X, E)W_{\text{in}})W_{\text{out}}$
- Randomly initialized neural network, additive (NN additive): $y = \text{Tanh}(XW_{\text{in}})W_{\text{out}} + E$

Root causal mechanisms, noise variables, and interventional distributions maintained the Dcdi defaults.

- Root causal mechanisms were set to Uniform$(-2, 2)$.
- Noise was set to $E \sim 0.4 \cdot \mathcal{N}(0, \sigma^2)$ where $\sigma^2 \sim \text{Uniform}(1, 2)$.
- Interventions were applied to all nodes (one at a time) by setting their causal mechanisms to $\mathcal{N}(0, 1)$.

Ablation datasets with $N > 100$ nodes contained 100,000 points each (same as $N = 100$). We set random seeds for each dataset using the hash of the output filename.

B.2 Baseline details

We considered the following baselines. All baselines were run using official implementations published by the authors.

Dcdi (Brouillard et al., 2020) was trained on each of the $N = 10, 20$ datasets using their published hyperparameters. We denote the Gaussian and Deep Sigmoidal Flow versions as DCDI-G and DCDI-DSF respectively. DCDI could not scale to graphs with $N = 100$ due to memory constraints (did not fit on a 32GB V100 GPU).

DCD-FG (Lopez et al., 2022) was trained on all of the test datasets using their published hyperparameters. We set the number of factors to $5, 10, 20$ for each of $N = 10, 20, 100$, based on their ablation studies. Due to numerical instability on $N = 100$, we clamped augmented Lagrangian multipliers μ and γ to 10 and stopped training if elements of the learned adjacency matrix reached `NaN` values. After discussion with the authors, we also tried adjusting the μ multiplier from 2 to 1.1, but the model did not converge within 48 hours.

DECI (Geffner et al., 2022) was trained on all of the test datasets using their published hyperparameters. However, on all $N = 100$ cases, the model failed to produce any meaningful results (adjacency matrices nearly all remained 0s with AUCs of 0.5). Thus, we only report results on $N = 10, 20$.

DiffAN (Sanchez et al., 2023) was trained on the each of the $N = 10, 20$ datasets using their published hyperparameters. The authors write that "most hyperparameters are hard-coded into [the] constructor of the DiffAN class and we verified they work across a wide set of datasets." We used the original, non-approximation version of their algorithm by maintaining `residue=True` in their codebase. We were unable to consistently run DiffAN with both R and GPU support within a Docker container, and the authors did not respond to questions regarding reproducibility, so all models were trained on the CPU only. We observed approximately a 10x speedup in the < 5 cases that were able to complete running on the GPU.

AVICI (Lorch et al., 2022) was run on all test datasets using the authors' pretrained `scm-v0` model, recommended for "arbitrary real-valued data." Note that this model is different from the models described in their paper (denoted Avici-L and Avici-R), as it was trained on *all* of their synthetic data, including test sets. We sampled 1000 observations per dataset uniformly at random, with their respective interventions (the maximum number of synthetic samples used in their original paper), except for Sachs, which used the entire dataset (as in their paper). Though the authors provided separate weights for synthetic mRNA data, we were unable to use it since we did not preserve the raw gene counts in our simulated mRNA datasets.

InvCov computes inverse covariance over 1000 examples. This does *not* orient edges, but it is a strong connectivity baseline. We discretize based on ground truth positive rate.

Corr and **D-Corr** are computed similarly, using global correlation and distance correlation, respectively (See C.1 for details).

B.3 Neural network design

Hyperparameters and architectural choices were selected by training the model on 20% of the the training and validation data for approximately 50k steps (several hours). We considered the following parameters in sequence.

- learned positional embedding vs. sinusoidal positional embedding
- number of layers × number of heads: $\{4, 8\} \times \{4, 8\}$
- learning rate $\eta = \{1e-4, 5e-5, 1e-5\}$

For our final model, we selected learned positional embeddings, 4 layers, 8 heads, and learning rate $\eta = 1e-4$.

Some empirical limitations of our implementations include: 1) a hard-coded maximum of 1000 variables (arbitrary), 2) generalize poorly to synthetic cyclic data, 3) err on the side of sparsity on real data, 4) inverse covariance can be numerically unstable on larger graphs (recommend models finetuned for correlation here), and 5) training requires full precision. These are artifacts of our training set and design choices.

B.4 Training and hardware details

The models were trained across 2 NVIDIA RTX A6000 GPUs and 60 CPU cores. We used the GPU exclusively for running the aggregator, and retained all classical algorithm execution on the CPUs (during data loading). The total pretraining time took approximately 14 hours for the final FCI model and 16 hours for the final GIES model.

For finetuning, we used rank $r = 2$ adapters on the axial attention model's key, query, and feedforward weights (Hu et al., 2022). We trained until convergence on the validation set (no improvement for 100 epochs), which took 4-6 hours with 40 CPUs and around 10 hours with 20 CPUs. We used a single NVIDIA RTX A6000 GPU, but the bottleneck was CPU availability.

For the scope of this paper, our models and datasets are fairly small. We did not scale further due to hardware constraints. Our primary bottlenecks to scaling up lay in availability of CPU cores and networking speed across nodes, rather than GPU memory or utilization. The optimal CPU:GPU ratio for Sea ranges from 20:1 to 40:1.

We are able to run inference comfortably over $N = 500$ graphs with $T = 500$ subsets of $k = 5$ nodes each, on a single 32GB V100 GPU. For runtime analysis, we used a batch size of 1, with 1 data worker per dataset. Our runtime could be further improved if we amortized the GPU utilization across batches.

B.5 Choice of classical causal discovery algorithm

For training, we selected FCI (Spirtes et al., 1995) as the underlying discovery algorithm in the observational setting over GES (Chickering, 2002), GRaSP (Lam et al., 2022), and LiNGAM (Shimizu et al., 2006) due to its speed and superior downstream performance. We hypothesize this may be due to its richer output (ancestral graph) providing more signal to the Transformer model. We also tried Causal Additive Models (Bühlmann et al., 2014), but its runtime was too slow for consistent GPU utilization. Observational algorithm implementations were provided by the causal-learn library (Zheng et al., 2023). The code for running these alternative classical algorithms is available in our codebase.

We selected GIES as the discovery algorithm in the interventional setting because an efficient Python implementation was readily available at `https://github.com/juangamella/gies`.

We tried incorporating implementations from the Causal Discovery Toolbox via a Docker image (Kalainathan et al., 2020), but there was excessive overhead associated with calling an R subroutine and reading/writing the inputs/results from disk.

Finally, we considered other independence tests for richer characterization, such as kernel-based methods. However, due to speed, we chose to remain with the default Fisherz conditional independence test for FCI, and BIC for GIES (Schwarz, 1978).

B.6 Sampling procedure

Selection scores: We consider three strategies for computing selection scores α. We include an empirical comparison of these strategies in Table 9.

1. Random selection: α is an $N \times N$ matrix of ones.
2. Global-statistic-based selection: $\alpha = \rho$.
3. Uncertainty-based selection: $\alpha = \hat{H}(E_t)$, where H denotes the information entropy

$$\alpha_{i,j} = - \sum_{e \in \{0,1,2\}} p(e) \log p(e). \tag{37}$$

Let $c^t_{i,j}$ be the number of times edge (i,j) was selected in $S_1 \dots S_{t-1}$, and let $\alpha^t = \alpha / \sqrt{c^t_{i,j}}$. We consider two strategies for selecting S_t based on α_t.

Greedy selection: Throughout our experiments, we used a greedy algorithm for subset selection. We normalize probabilities to 1 before the constructing each Categorical. Initialize

$$S_t \leftarrow \{i : i \sim \text{Categorical}(\alpha^t_1 \dots \alpha^t_N)\}. \tag{38}$$

where $\alpha^t_i = \sum_{j \neq i \in V} \alpha^t_{i,j}$. While $|S_t| < k$, update

$$S_t \leftarrow S_t \cup \{j : j \sim \text{Categorical}(\alpha^t_{1,S_t} \dots \alpha^t_{N,S_t})) \tag{39}$$

where

$$\alpha_{j,S_t} = \begin{cases} \sum_{i \in S_t} \alpha^t_{i,j} & j \notin S_t \\ 0 & \text{otherwise.} \end{cases} \tag{40}$$

Subset selection: We also considered the following subset-level selection procedure, and observed minor performance gain for significantly longer runtime (linear program takes around 1 second per batch). Therefore, we opted for the greedy method instead.

We solve the following integer linear program to select a subset S_t of size k that maximizes $\sum_{i \in S_t} \alpha^t_{i,j}$. Let $\nu_i \in \{0,1\}$ denote the selection of node i, and let $\epsilon_{i,j} \in \{0,1\}$ denote the selection of edge (i,j). Our objective is to

$$\begin{array}{lll} \text{maximize} & \sum_{i,j} a^t_{i,j} \cdot \epsilon_{i,j} & \\ \text{subject to} & \sum_i \nu_i = k & \text{subset size} \\ & \epsilon_{i,j} \geq \nu_i + \nu_j - 1 & \text{node-edge consistency} \\ & \epsilon_{i,j} \leq \nu_i & \\ & \epsilon_{i,j} \leq \nu_j, & \\ & \nu_i \in \{0,1\} & \\ & \epsilon_{i,j} \in \{0,1\} & \end{array}$$

for $i,j \in V \times V$, $i \in V$. S_t is the set of non-zero indices in ν.

The final algorithm used the greedy selection strategy, with the first half of batches sampled according to global statistics, and the latter half sampled randomly, with visit counts shared. This strategy was selected heuristically, and we did not observe significant improvements or drops in performance when switching to other strategies (e.g. all greedy statistics-based, greedy uncertainty-based, linear program uncertainty-based, etc.)

Table 9 compares the heuristics-based greedy sampler (inverse covariance + random) with the model uncertainty-based greedy sampler. Runtimes are plotted in Figure 6. The latter was run on CPU only, since

Table 9: Comparison between heuristics-based sampler (random and inverse covariance) vs. model confidence-based sampler. The suffix -L indicates the greedy confidence-based sampler. Each setting encompasses 5 distinct Erdős-Rényi graphs. The symbol † indicates that SEA was not pretrained on this setting. Bold indicates best of all models considered (including baselines not pictured).

N	E	Model	Linear			NN add.			NN non-add.			Sigmoid†			Polynomial†		
			mAP↑	OA↑	shd↓	mAP↑	OA↑	shd↓	mAP↑	OA↑	shd↓	mAP↑	OA↑	shd↓	mAP↑	OA↑	shd↓
10	10	SEA-F	0.97	0.92	1.6	**0.95**	**0.92**	2.4	**0.92**	0.94	2.8	0.83	0.76	3.7	0.69	0.71	6.7
		SEA-G	**0.99**	**0.94**	1.2	0.94	0.88	2.6	0.91	0.93	3.2	0.85	0.84	4.0	0.70	0.79	**5.8**
		SEA-F-L	0.97	0.93	**1.0**	0.95	0.87	2.4	**0.92**	**0.98**	3.4	0.84	0.77	3.9	**0.70**	0.79	**5.8**
		SEA-G-L	0.98	0.93	1.4	0.94	0.91	2.8	0.91	0.94	4.0	**0.88**	**0.84**	**3.6**	0.70	**0.80**	**5.8**
10	40	SEA-F	0.90	0.87	14.4	0.91	0.94	11.2	0.87	0.86	16.0	**0.81**	0.85	22.7	0.81	0.92	33.4
		SEA-G	**0.94**	**0.91**	**12.8**	0.91	**0.95**	**10.4**	**0.89**	**0.89**	17.2	0.81	**0.87**	24.5	0.89	0.93	29.5
		SEA-F-L	0.91	0.90	15.6	**0.91**	0.92	15.8	0.88	0.86	14.2	0.81	0.84	23.2	0.82	0.93	33.8
		SEA-G-L	0.93	0.91	13.4	0.91	0.93	**10.4**	0.88	0.85	16.2	0.79	0.83	25.5	**0.90**	**0.94**	28.3
20	20	SEA-F	0.97	0.92	3.2	0.94	0.97	3.2	0.84	0.93	7.2	0.84	0.85	7.6	**0.71**	**0.80**	10.2
		SEA-G	0.97	0.89	3.0	**0.94**	0.95	3.4	0.83	0.94	7.8	0.84	0.83	8.1	0.69	0.78	10.1
		SEA-F-L	0.97	**0.92**	2.8	0.93	0.95	3.8	**0.85**	0.94	6.8	**0.85**	0.85	**7.5**	0.67	0.78	**9.9**
		SEA-G-L	**0.97**	0.90	**2.6**	**0.94**	**0.98**	3.4	0.83	**0.97**	7.0	0.84	0.84	7.9	0.67	0.79	10.6
20	80	SEA-F	0.86	**0.93**	29.6	0.55	0.90	73.6	0.72	**0.93**	51.8	**0.77**	0.85	42.8	0.61	0.89	61.8
		SEA-G	**0.89**	0.92	**26.8**	**0.58**	0.88	71.4	0.73	0.92	50.6	0.76	0.84	45.0	**0.65**	**0.89**	60.1
		SEA-F-L	0.86	0.92	32.0	0.55	**0.90**	74.0	0.74	0.93	49.2	0.76	**0.87**	**41.8**	0.59	0.88	62.3
		SEA-G-L	**0.89**	0.92	28.4	0.58	0.89	71.6	0.75	0.92	49.4	0.75	0.85	45.7	**0.65**	0.88	60.6

it was non-trivial to access the GPU within a PyTorch data loader. We ran a forward pass to obtain an updated selection score every 10 batches, so this accrued over 10 times the number of forward passes, all on CPU. With proper engineering, this model-based sampler is expected to be much more efficient than reported. Still, it is faster than nearly all baselines.

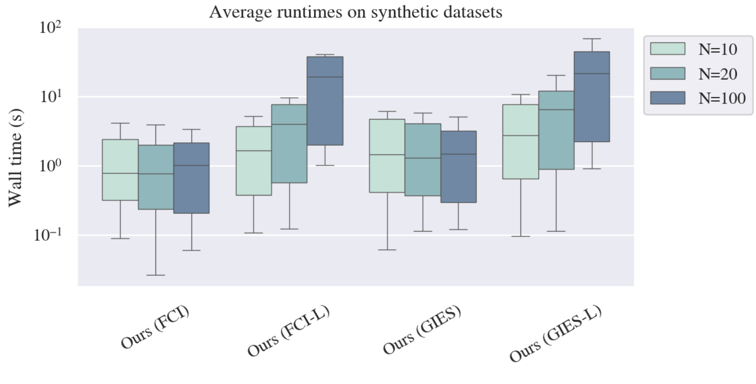

Figure 6: Runtime for heuristics-based greedy sampler vs. model uncertainty-based greedy sampler (suffix -L). For sampling, the model was run on CPU only, due to the difficulty of invoking GPU in the PyTorch data sampler.

B.7 Limitations

There are several aspects of this work that could be further improved in future iterations. First, classical causal discovery algorithms make different types of errors, and different summary statistics capture distinct aspects of data. Incorporating this diversity at training time remains unexplored, both from experimental and theoretical perspectives. The empirical success of this approach also motivates further theoretical studies into amortized and supervised causal discovery algorithms, especially with regards to finite data regimes. Finally, while our synthetic datasets were quite substantial, dynamically generating them during the training process (as Lorch et al. (2022) does) may lead to even better generalization, as the model is unlikely to see the same dataset twice.

C Additional analyses

C.1 Choice of global statistic

We selected inverse covariance as our global feature due to its ease of computation and its relationship to partial correlation. For context, we also provide the performance analysis of several alternatives. Tables 11 and 12 compare the results of different graph-level statistics on our synthetic datasets. Discretization thresholds for SHD were obtained by computing the p^{th} quantile of the computed values, where $p = 1-(E/N)$. This is not entirely fair, as no other baseline receives the same calibration, but these ablation studies only seek to compare state-of-the-art causal discovery methods with the "best" possible (oracle) statistical alternatives.

Corr refers to global correlation,

$$\rho_{i,j} = \frac{\mathbb{E}\left(X_i X_j\right) - \mathbb{E}\left(X_i\right)\mathbb{E}\left(X_j\right)}{\sqrt{\mathbb{E}\left(X_i^2\right) - \mathbb{E}\left(X_i\right)^2} \cdot \sqrt{\mathbb{E}\left(X_j^2\right) - \mathbb{E}\left(X_j\right)^2}}. \tag{41}$$

D-Corr refers to distance correlation, computed between all pairs of variables. Distance correlation captures both linear and non-linear dependencies, and $\text{D-C}\textsc{orr}(X_i, X_j) = 0$ if and only if $X_i \perp\!\!\!\perp X_j$. Please refer to Sz'ekely et al. (2007) for the full derivation. Despite its power to capture non-linear dependencies, we opted not to use D-Corr because it is quite slow to compute between all pairs of variables.

InvCov refers to inverse covariance, computed globally,

$$\rho = \mathbb{E}\left((X - \mathbb{E}\left(X\right))(X - \mathbb{E}\left(X\right))^T\right)^{-1}. \tag{42}$$

For graphs $N < 100$, inverse covariance was computed directly using NumPy. For graphs $N \geq 100$, inverse covariance was computed using Ledoit-Wolf shrinkage at inference time Ledoit & Wolf (2004). Unfortunately we only realized this after training our models, so swapping to Ledoit-Wolf leads to some distribution shift (and drop in performance) on Sea results for large graphs.

C.2 Results on simulated mRNA data

We generated mRNA data using the SERGIO simulator Dibaeinia & Sinha (2020). We sampled datasets with the Hill coefficient set to $\{0.25, 0.5, 1, 2, 4\}$ for training, and 2 for testing (2 was default). We set the decay rate to the default 0.8, and the noise parameter to the default of 1.0. We sampled 400 graphs for each of $N = \{10, 20\}$ and $E = \{N, 2N\}$.

These data distributions are quite different from typical synthetic datasets, as they simulate steady-state measurements and the data are lower bounded at 0 (gene counts). Thus, we trained a separate model on these data using the Sea (Fci) architecture. Table 13 shows that Sea performs best across the board.

C.3 Results and ablation studies on synthetic data

For completeness, we include additional results and analysis on the synthetic datasets. Tables 17 and 18 compare all baselines across all metrics and graph sizes on Erdős-Rényi graphs. Tables 19 and 20 include the same evaluation on scale-free graphs. Tables 21 and 22 assess $N = 100$ graphs.

Table 15 ablates the contribution of the global and marginal features by setting their hidden representations to zero. Note that our model has never seen this type of input during training, so drops in performance may be conflated with input distributional shift. Overall, removing the joint statistics ($h^\rho \leftarrow 0$) leads to a higher

Table 10: Synthetic experiments, edge direction accuracy (higher is better). All standard deviations were within 0.2. The symbol † indicates that Sea was not pretrained on this setting.

N	E	Model	Linear	NN add	NN	Sig.†	Poly.†
10	10	Dcdi-G	0.74	0.80	0.85	0.41	0.44
		Dcdi-Dsf	0.79	0.62	0.68	0.38	0.39
		Dcd-Fg	0.50	0.47	0.70	0.43	0.54
		DiffAn	0.61	0.55	0.26	0.53	0.47
		Deci	0.50	0.43	0.62	0.63	0.75
		Avici	0.80	**0.92**	0.83	0.81	0.75
		Fci-Avg	0.52	0.43	0.41	0.55	0.40
		Gies-Avg	0.76	0.49	0.69	0.67	0.63
		Sea (Fci)	0.92	**0.92**	**0.94**	0.76	0.71
		Sea (Gies)	**0.94**	0.88	0.93	**0.84**	**0.79**
20	80	Dcdi-G	0.47	0.43	0.82	0.40	0.24
		Dcdi-Dsf	0.50	0.49	0.78	0.41	0.28
		Dcd-Fg	0.58	0.65	0.75	0.62	0.48
		DiffAn	0.46	0.28	0.36	0.45	0.21
		Deci	0.30	0.47	0.35	0.48	0.57
		Avici	0.57	0.67	0.74	0.63	0.62
		Fci-Avg	0.19	0.19	0.22	0.33	0.23
		Gies-Avg	0.56	0.73	0.59	0.62	0.61
		Sea (Fci)	**0.93**	**0.90**	**0.93**	**0.85**	**0.89**
		Sea (Gies)	0.92	0.88	0.92	0.84	**0.89**
100	400	Dcd-Fg	0.46	0.60	0.70	0.67	0.53
		Avici	0.61	0.68	0.72	0.54	0.42
		Sea (Fci)	0.93	0.90	0.91	**0.87**	0.82
		Sea (Gies)	**0.94**	**0.91**	**0.92**	**0.87**	**0.84**

Table 11: Comparison of global statistics (continuous metrics). All standard deviations within 0.1.

N	E	Model	Linear		NN add.		NN non-add.		Sigmoid		Polynomial	
			mAP ↑	AUC ↑	mAP ↑	AUC ↑	mAP ↑	AUC ↑	mAP ↑	AUC ↑	mAP ↑	AUC ↑
10	10	Corr	0.45	0.87	0.41	0.86	0.41	0.85	0.46	0.86	0.45	0.85
		D-Corr	0.42	0.86	0.41	0.87	0.40	0.87	0.43	0.86	0.45	0.89
		InvCov	0.49	0.87	0.45	0.86	0.36	0.81	0.44	0.86	0.45	0.83
10	40	Corr	0.47	0.53	0.47	0.52	0.46	0.52	0.48	0.53	0.48	0.54
		D-Corr	0.46	0.53	0.46	0.51	0.46	0.54	0.48	0.53	0.47	0.54
		InvCov	0.50	0.57	0.48	0.52	0.47	0.53	0.47	0.50	0.48	0.52
100	100	Corr	0.42	0.99	0.25	0.94	0.25	0.93	0.42	0.98	0.35	0.91
		D-Corr	0.41	0.99	0.25	0.96	0.26	0.96	0.41	0.98	0.37	0.94
		InvCov	0.40	0.99	0.22	0.94	0.16	0.87	0.40	0.97	0.36	0.90
100	400	Corr	0.19	0.80	0.10	0.63	0.14	0.72	0.27	0.84	0.20	0.72
		D-Corr	0.19	0.80	0.10	0.63	0.14	0.75	0.26	0.84	0.21	0.74
		InvCov	0.25	0.91	0.09	0.62	0.14	0.77	0.27	0.86	0.20	0.67

performance drop than removing the marginal estimates ($h^E \leftarrow 0$). However, the gap between these ablation studies and our final performance may be quite large in some cases, so both inputs are important to the prediction.

Table 12: Comparison of global statistics (SHD). Discretization thresholds for SHD were obtained by computing the p^{th} quantile of the computed values, where $p = 1 - (E/N)$.

N	E	Model	Linear	NN add.	NN non-add.	Sigmoid	Polynomial
10	10	Corr	10.6±2.8	10.2±4.6	12.0±1.9	11.1±4.3	9.9±2.8
		D-Corr	10.4±2.6	9.8±4.7	12.2±2.6	10.8±3.3	10.2±3.2
		InvCov	11.0±2.8	11.4±5.5	13.6±2.9	11.4±4.1	10.9±3.5
10	40	Corr	39.2±2.4	38.0±1.8	38.2±0.7	38.8±3.3	38.2±2.0
		D-Corr	38.8±2.0	38.8±1.5	37.0±0.6	38.9±3.2	38.0±2.0
		InvCov	35.8±2.3	39.2±1.5	37.6±2.7	40.7±2.2	38.4±1.2
100	100	Corr	113.0±4.9	132.2±18.0	144.6±5.2	106.5±11.5	110.3±6.1
		D-Corr	113.8±5.3	133.2±17.9	144.2±6.7	108.5±11.9	109.5±5.7
		InvCov	124.4±8.1	130.0±17.2	158.8±6.2	112.3±14.8	106.3±4.6
100	400	Corr	580.4±24.5	666.0±13.5	626.2±23.4	516.5±18.5	562.5±20.1
		D-Corr	578.2±24.7	665.4±15.4	626.6±21.9	522.3±17.6	557.2±20.4
		InvCov	557.0±11.7	667.8±15.4	639.0±9.7	514.7±23.1	539.4±18.4

Table 13: Causal discovery results on simulated mRNA data. Each setting encompasses 5 distinct scale-free graphs. Data were generated via SERGIO Dibaeinia & Sinha (2020).

N	E	Model	mAP ↑	AUC ↑	SHD ↓	OA ↑
10	10	Dcdi-G	0.48±0.1	0.73±0.1	16.1±3.3	0.59±0.2
		Dcdi-Dsf	0.63±0.1	0.84±0.1	18.5±2.7	0.79±0.2
		Dcd-Fg	0.59±0.2	0.82±0.1	81.0±0.0	0.79±0.2
		Avici	0.58±0.2	0.85±0.1	6.4±4.7	0.72±0.2
		Sea (Fci)	**0.92**±0.1	**0.98**±0.0	**1.9**±2.0	**0.92**±0.1
10	20	Dcdi-G	0.32±0.1	0.57±0.1	26.2±1.3	0.47±0.2
		Dcdi-Dsf	0.44±0.1	0.64±0.1	25.7±1.3	0.63±0.1
		Dcd-Fg	0.43±0.1	0.69±0.1	73.0±0.0	0.67±0.2
		Avici	0.22±0.1	0.44±0.2	16.8±1.5	0.27±0.3
		Sea (Fci)	**0.76**±0.1	**0.90**±0.1	**8.8**±1.5	**0.85**±0.1
20	20	Dcdi-G	0.48±0.1	0.86±0.1	37.3±2.8	0.65±0.1
		Dcdi-Dsf	0.45±0.1	0.92±0.0	51.9±15.8	0.81±0.1
		Dcd-Fg	0.34±0.2	0.87±0.0	361±0	0.66±0.2
		Avici	0.32±0.2	0.78±0.1	18.7±4.9	0.66±0.2
		Sea (Fci)	**0.54**±0.2	**0.94**±0.0	**16.6**±3.3	**0.83**±0.1
20	40	Dcdi-G	0.31±0.1	0.65±0.1	54.7±2.7	0.49±0.1
		Dcdi-Dsf	0.40±0.1	0.71±0.1	54.6±4.4	0.63±0.1
		Dcd-Fg	0.36±0.1	0.77±0.1	343±0	0.67±0.1
		Avici	0.17±0.1	0.54±0.1	37.1±1.9	0.46±0.1
		Sea (Fci)	**0.50**±0.1	**0.85**±0.1	**31.4**±4.9	**0.78**±0.1

Table 16 shows that despite omitting the DAG constraint, we find that our predicted graphs (test split) are nearly all acyclic, with a naive discretization threshold of 0.5. Unlike Lippe et al. (2022), which also omits the acyclicity constraint during training but optionally enforces it at inference time, we do not require any post-processing to achieve high performance. Empirically, we found existing DAG constraints to be unstable (Lagrangian) and slow to optimize (Zheng et al., 2018; Brouillard et al., 2020). DAG behavior would not emerge until late in training, when the regularization term is of 1e-8 scale or smaller.

Table 14: Scaling to synthetic graphs, larger than those seen in training. Each setting encompasses 5 distinct Erdős-Rényi graphs. All Sea runs in this table used $T = 500$ subsets of nodes, with $b = 500$ examples per batch. For Avici, we took $M = 2000$ samples per dataset (higher than maximum analyzed in their paper), since it performed better than $M = 1000$. Here, the mean AUC values are artificially high due to the high negative rates, as actual edges scale linearly as N, while the number of possible edges scales quadratically.

N	Model	Linear, $E = N$				Linear, $E = 4N$			
		mAP ↑	AUC ↑	SHD ↓	OA ↑	mAP ↑	AUC ↑	SHD ↓	OA ↑
100	InvCov	0.43±0.0	0.99±0.0	117±7	—	0.30±0.0	0.93±0.0	512±11	—
	Corr	0.42±0.0	0.99±0.0	113±5	—	0.19±0.0	0.80±0.0	579±25	—
	Avici	0.03±0.0	0.43±0.1	109±6	0.49±0.0	0.11±0.0	0.55±0.1	394±14	0.58±0.0
	Sea (Fci)	**0.97**±0.0	**1.00**±0.0	**11.6**±4.3	**0.93**±0.0	0.88±0.0	0.98±0.0	129±10	0.94±0.0
	Sea (Gies)	**0.97**±0.0	**1.00**±0.0	12.8±4.7	0.91±0.0	**0.91**±0.0	**0.99**±0.0	**105**±6	**0.95**±0.0
200	InvCov	0.45±0.0	1.00±0.0	218±11	—	0.33±0.0	0.96±0.0	1000±23	—
	Corr	0.42±0.0	0.99±0.0	223±8	—	0.18±0.0	0.86±0.0	1184±25	—
	Avici	0.00±0.0	0.36±0.1	207±10	0.41±0.1	0.05±0.0	0.53±0.1	827±37	0.54±0.1
	Sea (Fci)	0.91±0.0	**1.00**±0.0	49.9±5.4	0.87±0.0	0.82±0.0	0.97±0.0	327±52	0.92±0.0
	Sea (Gies)	**0.95**±0.0	**1.00**±0.0	**35.4**±5.7	**0.91**±0.0	**0.86**±0.0	**0.98**±0.0	**272**±50	**0.92**±0.0
300	InvCov	0.46±0.0	**1.00**±0.0	308±20	—	0.35±0.0	0.98±0.0	1445±56	—
	Corr	0.42±0.0	1.00±0.0	326±21	—	0.20±0.0	0.89±0.0	1710±82	—
	Avici	0.01±0.0	0.70±0.0	298±19	0.64±0.0	0.02±0.0	0.50±0.0	1214±68	0.51±0.0
	Sea (Fci)	0.80±0.0	1.00±0.0	121±14	0.78±0.0	0.70±0.0	0.95±0.0	693±67	0.86±0.0
	Sea (Gies)	**0.88**±0.0	**1.00**±0.0	**88.9**±11.3	**0.84**±0.0	**0.78**±0.0	**0.96**±0.0	**556**±71	**0.87**±0.0
400	InvCov	0.47±0.0	1.00±0.0	418±7	—	0.36±0.0	0.98±0.0	1883±28	—
	Corr	0.42±0.0	1.00±0.0	445±14	—	0.20±0.0	0.91±0.0	2269±52	—
	Avici	0.01±0.0	0.68±0.0	411±7	0.62±0.0	0.01±0.0	0.46±0.0	1614±21	0.47±0.0
	Sea (Fci)	0.49±0.2	0.93±0.1	314±107	0.61±0.1	0.56±0.1	0.90±0.1	1103±190	0.75±0.1
	Sea (Gies)	**0.70**±0.1	**0.99**±0.0	**226**±57	**0.71**±0.1	**0.70**±0.0	**0.94**±0.0	**872**±44	**0.80**±0.0
500	InvCov	0.47±0.0	1.00±0.0	504±19	—	0.38±0.0	0.99±0.0	2300±34	—
	Corr	0.42±0.0	1.00±0.0	543±18	—	0.21±0.0	0.93±0.0	2790±78	—
	Avici	0.00±0.0	0.70±0.0	497±19	**0.63**±0.0	0.01±0.0	0.48±0.0	2004±25	0.48±0.0
	Sea (Fci)	0.27±0.1	0.90±0.1	758±297	0.51±0.0	0.29±0.1	0.86±0.1	1824±273	0.56±0.1
	Sea (Gies)	**0.41**±0.2	**0.98**±0.0	**485**±170	0.57±0.1	**0.48**±0.1	**0.92**±0.0	**1654**±505	**0.67**±0.0

Alternatively, we could quantify the raw information content provided by these two features through the InvCov, Fci*, and Gies* baselines (Tables 17, 18, 19, 20). Overall, InvCov and Fci* are comparable to worse-performing baselines. Gies* performs very well, sometimes approaching the strongest baselines. However, there remains a large gap in performance between these ablations and our method, highlighting the value of learning non-linear transformations of these inputs.

Table 14 and Figure 8 show that the current implementations of Sea can generalize to graphs up to 4× larger than those seen during training. During training, we did not initially anticipate testing on much larger graphs. As a result, there are two minor issues with the current implementation with respect to scaling. First, we set an insufficient maximum subset positional embedding size of 500, so it was impossible to encode more subsets. Second, we did not sample random starting subset indices to ensure that higher-order embeddings are updated equally. Since we never sampled up to 500 subsets during training, these higher-order embeddings were essentially random. We anticipate that increasing the limit on the number of subsets and ensuring that

Table 15: Causal discovery ablations by setting hidden representations to zero. Each setting encompasses 5 distinct Erdős-Rényi graphs. The symbol † indicates that Sea was not pretrained on this setting. We set $T = 100$.

N	E	Model	Linear		NN add.		NN non-add.		Sigmoid†		Polynomial†	
			mAP ↑	SHD ↓	mAP ↑	SHD ↓	mAP ↑	SHD ↓	mAP ↑	SHD ↓	mAP ↑	SHD ↓
10	10	Sea (Fci)	0.97	1.6	0.95	2.4	0.92	2.8	0.83	3.7	0.69	6.7
		$h^\rho \leftarrow 0$	0.20	29.8	0.27	22.4	0.34	24.2	0.26	22.6	0.24	26.0
		$h^E \leftarrow 0$	0.61	24.0	0.71	28.8	0.76	27.8	0.49	26.7	0.51	26.7
		Sea (Gies)	0.99	1.2	0.94	2.6	0.91	3.2	0.85	4.0	0.70	5.8
		$h^\rho \leftarrow 0$	0.30	29.2	0.27	29.4	0.19	29.0	0.35	27.4	0.31	27.1
		$h^E \leftarrow 0$	0.85	6.4	0.82	10.2	0.78	13.2	0.63	10.2	0.55	13.4
20	80	Sea (Fci)	0.86	29.6	0.55	73.6	0.72	51.8	0.77	42.8	0.61	61.8
		$h^\rho \leftarrow 0$	0.23	128.4	0.27	110.6	0.22	119.6	0.23	110.7	0.23	111.1
		$h^E \leftarrow 0$	0.79	50.4	0.52	99.6	0.71	76.4	0.58	93.6	0.59	87.5
		Sea (Gies)	0.89	26.8	0.58	71.4	0.73	50.6	0.76	45.0	0.65	60.1
		$h^\rho \leftarrow 0$	0.25	125.2	0.21	123.0	0.24	113.6	0.27	118.0	0.24	129.8
		$h^E \leftarrow 0$	0.86	35.2	0.55	76.8	0.70	53.4	0.69	47.1	0.59	63.5
100	400	Sea (Fci)	0.90	122.0	0.28	361.2	0.60	273.2	0.69	226.9	0.38	327.0
		$h^\rho \leftarrow 0$	0.05	726.4	0.04	639.4	0.05	637.0	0.05	760.2	0.04	658.3
		$h^E \leftarrow 0$	0.82	167.4	0.04	403.4	0.51	352.4	0.64	263.8	0.33	366.1
		Sea (Gies)	0.91	116.6	0.27	364.4	0.61	266.8	0.69	218.3	0.38	328.0
		$h^\rho \leftarrow 0$	0.05	780.0	0.04	846.0	0.05	715.4	0.04	744.4	0.04	769.8
		$h^E \leftarrow 0$	0.86	134.8	0.03	403.4	0.52	357.8	0.67	224.1	0.32	359.6

Table 16: Our predicted graphs are highly acyclic, on synthetic ER test sets.

N	Acyclic	Total	Proportion
10	434	440	0.99
20	431	440	0.98
100	433	440	0.98

all embeddings are sufficiently learned will improve the generalization capacity on larger graphs. Nonetheless, our current model already obtains reasonable performance on larger graphs, out of the box.

Finally, we note that Avici scales very poorly to graphs significantly beyond the scope of their training set. For example, $N = 100$ is only 2× their largest training graphs, but the performance already drops dramatically.

Figure 7 depicts the model runtimes. Sea continues to run quickly on much larger graphs, while Avici runtimes increase significantly with graph size.

Dcdi learns a new generative model over each dataset, and its more powerful, deep sigmoidal flow variant seems to perform well in some (but not all) of these harder cases.

C.4 Results on real datasets

The Sachs flow cytometry dataset (Sachs et al., 2005) measured the expression of phosphoproteins and phospholipids at the single cell level. We use the subset proposed by Wang et al. (2017). The ground truth "consensus graph" consists of 11 nodes and 17 edges over 5,845 samples, of which 1,755 are observational and 4,091 are interventional. The observational data were generated by a "general perturbation" which activated signaling pathways, and the interventional data were generated by perturbations intended to target

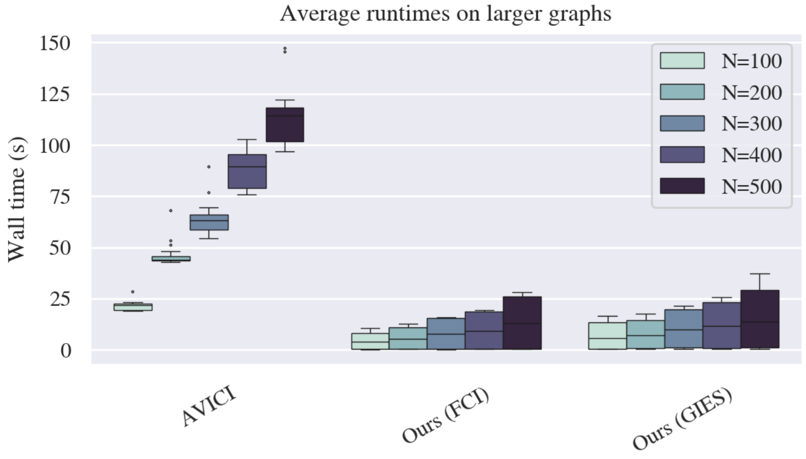

Figure 7: Sea scales very well in terms of runtime on much larger graphs, while Avici runtimes suffer as graph sizes increase.

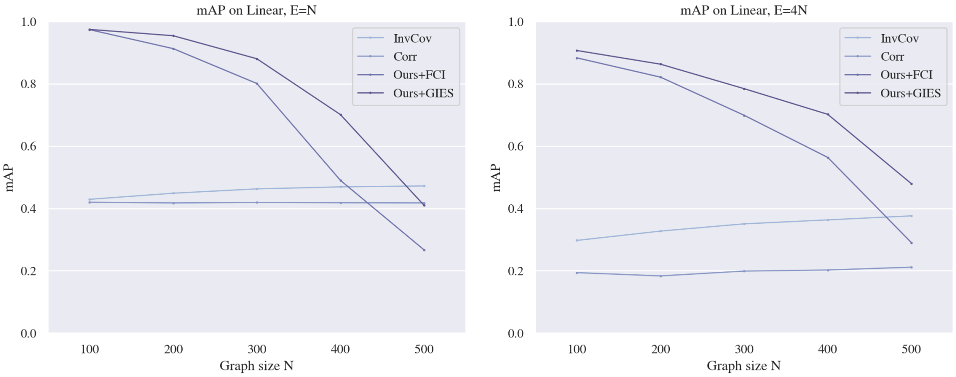

Figure 8: mAP on graphs larger than seen during training. During training, we only sampled a maximum of 100 subsets, so performance drop may be due to extrapolation beyond trained embeddings. We did not have time to finetune these embeddings for more samples. These values correspond to the numbers in Table 14.

individual proteins. Despite the popularity of this dataset in causal discovery literature (due to lack of better alternatives), biological networks are known to be time-resolved and cyclic, so the validity of the ground truth "consensus" graph has been questioned by experts Mooij et al. (2020). Nonetheless, we benchmark all methods on this dataset in Table 23.

Table 17: Full results on synthetic datasets (continuous metrics). Mean/std over 5 distinct Erdős-Rényi graphs. † indicates o.o.d. setting. ∗ indicates non-parametric bootstrapping. All standard deviations within 0.03 (most within 0.01).

N	E	Model	Linear		NN add.		NN non-add.		Sigmoid†		Polynomial†	
			mAP ↑	AUC ↑	mAP ↑	AUC ↑	mAP ↑	AUC ↑	mAP ↑	AUC ↑	mAP ↑	AUC ↑
10	10	Dcdi-G	0.74	0.88	0.79	0.91	0.89	0.95	0.46	0.72	0.41	0.68
		Dcdi-Dsf	0.82	0.92	0.57	0.83	0.50	0.81	0.38	0.69	0.29	0.64
		Dcd-Fg	0.45	0.68	0.41	0.67	0.59	0.79	0.40	0.64	0.50	0.72
		DiffAn	0.25	0.73	0.32	0.70	0.12	0.51	0.24	0.70	0.20	0.65
		Deci	0.18	0.63	0.16	0.63	0.23	0.71	0.29	0.72	0.46	0.83
		Avici	0.45	0.80	0.81	0.97	0.65	0.89	0.52	0.81	0.31	0.70
		VarSort*	0.70	0.84	0.76	0.90	0.83	0.93	0.52	0.72	0.40	0.71
		InvCov	0.46	0.88	0.43	0.86	0.34	0.81	0.43	0.86	0.43	0.83
		Fci*	0.52	0.78	0.38	0.71	0.40	0.70	0.56	0.79	0.41	0.71
		Gies*	0.81	0.96	0.61	0.93	0.71	0.92	0.70	0.95	0.61	0.87
		Sea (Fci)	0.98	1.00	0.88	0.98	0.88	0.97	0.83	**0.97**	0.62	0.88
		Sea (Gies)	**0.99**	**1.00**	**0.94**	**0.99**	**0.91**	**0.98**	**0.85**	0.97	**0.70**	**0.89**
10	40	Dcdi-G	0.65	0.72	0.65	0.74	0.84	0.88	0.54	0.59	0.56	0.61
		Dcdi-Dsf	0.65	0.72	0.59	0.67	0.84	0.90	0.52	0.58	0.57	0.62
		Dcd-Fg	0.51	0.57	0.57	0.63	0.53	0.59	0.65	0.68	0.65	0.68
		DiffAn	0.40	0.49	0.36	0.37	0.41	0.53	0.40	0.45	0.37	0.40
		Deci	0.45	0.49	0.50	0.58	0.44	0.52	0.53	0.61	0.63	0.72
		Avici	0.46	0.47	0.63	0.65	0.79	0.86	0.49	0.53	0.47	0.55
		VarSort*	0.81	0.83	0.87	0.89	0.71	0.73	0.69	0.72	0.56	0.62
		InvCov	0.49	0.57	0.46	0.50	0.46	0.53	0.47	0.50	0.48	0.53
		Fci*	0.43	0.50	0.50	0.53	0.46	0.52	0.50	0.51	0.45	0.50
		Gies*	0.49	0.53	0.56	0.64	0.49	0.53	0.44	0.46	0.61	0.62
		Sea (Fci)	0.83	0.85	0.85	0.89	0.86	0.90	0.74	0.75	0.69	0.67
		Sea (Gies)	**0.94**	**0.95**	**0.91**	**0.94**	**0.89**	**0.92**	**0.81**	**0.85**	**0.89**	**0.92**
20	20	Dcdi-G	0.59	0.87	0.78	0.94	0.75	0.91	0.36	0.81	0.42	0.74
		Dcdi-Dsf	0.66	0.89	0.69	0.91	0.41	0.83	0.37	0.82	0.26	0.71
		Dcd-Fg	0.48	0.85	0.58	0.91	0.51	0.87	0.50	0.78	0.44	0.76
		DiffAn	0.19	0.73	0.16	0.69	0.20	0.72	0.29	0.79	0.09	0.65
		Deci	0.14	0.70	0.14	0.72	0.16	0.73	0.24	0.79	0.35	0.84
		Avici	0.48	0.87	0.59	0.91	0.67	0.90	0.42	0.84	0.24	0.69
		VarSort*	0.81	0.91	0.81	0.92	0.57	0.83	0.50	0.76	0.33	0.69
		InvCov	0.40	0.90	0.31	0.90	0.31	0.84	0.42	0.92	0.41	0.87
		Fci*	0.66	0.86	0.42	0.74	0.40	0.77	0.56	0.80	0.41	0.76
		Gies*	0.84	0.99	0.79	0.97	0.56	0.93	0.71	0.97	0.62	0.91
		Sea (Fci)	0.96	**1.00**	0.91	0.99	0.82	**0.97**	**0.85**	**0.98**	**0.69**	0.91
		Sea (Gies)	**0.97**	**1.00**	**0.94**	**0.99**	**0.83**	0.97	0.84	0.97	0.69	**0.92**
20	80	Dcdi-G	0.46	0.73	0.41	0.71	**0.82**	**0.93**	0.48	0.71	0.37	0.62
		Dcdi-Dsf	0.48	0.75	0.44	0.74	0.74	0.92	0.48	0.71	0.38	0.63
		Dcd-Fg	0.32	0.61	0.33	0.64	0.41	0.73	0.47	0.74	0.49	0.69
		DiffAn	0.21	0.53	0.19	0.41	0.18	0.46	0.22	0.55	0.18	0.37
		Deci	0.25	0.57	0.29	0.61	0.26	0.59	0.31	0.66	0.43	0.73
		Avici	0.34	0.63	0.46	0.73	0.49	0.74	0.34	0.64	0.30	0.59
		VarSort*	0.76	0.86	0.50	0.81	0.47	0.69	0.59	0.76	0.38	0.63
		InvCov	0.36	0.72	0.26	0.54	0.30	0.64	0.35	0.72	0.32	0.61
		Fci*	0.30	0.59	0.31	0.57	0.30	0.59	0.41	0.66	0.34	0.61
		Gies*	0.41	0.75	0.44	0.74	0.46	0.73	0.50	0.78	0.49	0.69
		Sea (Fci)	0.80	0.92	0.55	0.81	0.70	0.89	0.74	0.85	0.55	0.67
		Sea (Gies)	**0.89**	**0.95**	**0.58**	**0.84**	0.73	0.90	**0.76**	**0.90**	**0.65**	**0.84**

Table 18: Full results on synthetic datasets (discrete metrics). Mean/std over 5 distinct Erdős-Rényi graphs. † indicates o.o.d. setting. ∗ indicates non-parametric bootstrapping. All OA standard deviations within 0.2.

N	E	Model	Linear		NN add.		NN non-add.		Sigmoid†		Polynomial†	
			OA ↑	SHD ↓	OA ↑	SHD ↓	OA ↑	SHD ↓	OA ↑	SHD ↓	OA ↑	SHD ↓
10	10	DCDI-G	0.73	2.8$_{\pm2}$	0.84	**2.2**$_{\pm3}$	0.88	**1.0**$_{\pm1}$	0.46	5.8$_{\pm3}$	0.33	8.9$_{\pm6}$
		DCDI-DSF	0.81	2.0$_{\pm3}$	0.73	3.0$_{\pm3}$	0.60	4.2$_{\pm1}$	0.43	6.3$_{\pm3}$	0.24	11.2$_{\pm5}$
		DCD-FG	0.50	20.4$_{\pm3}$	0.47	21.2$_{\pm4}$	0.70	19.2$_{\pm4}$	0.43	19.8$_{\pm4}$	0.54	18.5$_{\pm5}$
		DiffAn	0.61	14.0$_{\pm5}$	0.55	13.6$_{\pm14}$	0.26	21.8$_{\pm8}$	0.53	12.0$_{\pm5}$	0.47	15.0$_{\pm6}$
		DECI	0.50	19.4$_{\pm5}$	0.43	13.8$_{\pm6}$	0.62	16.2$_{\pm3}$	0.63	13.9$_{\pm7}$	0.75	7.8$_{\pm4}$
		AVICI	0.58	8.2$_{\pm4}$	0.79	4.2$_{\pm3}$	0.65	5.6$_{\pm3}$	0.54	8.3$_{\pm3}$	0.35	9.6$_{\pm4}$
		VarSort*	0.70	6.0$_{\pm2}$	0.74	4.0$_{\pm2}$	0.90	4.2$_{\pm3}$	0.52	7.6$_{\pm3}$	0.48	9.3$_{\pm3}$
		InvCov	—	10.6$_{\pm3}$	—	10.2$_{\pm6}$	—	13.6$_{\pm3}$	—	11.1$_{\pm4}$	—	10.4$_{\pm3}$
		FCI*	0.52	10.0$_{\pm3}$	0.43	8.2$_{\pm4}$	0.41	9.8$_{\pm2}$	0.55	9.1$_{\pm3}$	0.40	10.0$_{\pm4}$
		GIES*	0.76	3.6$_{\pm2}$	0.49	6.0$_{\pm5}$	0.69	4.8$_{\pm2}$	0.67	5.9$_{\pm3}$	0.63	7.1$_{\pm3}$
		SEA (FCI)	0.93	**1.0**$_{\pm1}$	0.82	3.0$_{\pm4}$	0.90	3.8$_{\pm2}$	0.73	**3.9**$_{\pm2}$	0.70	6.1$_{\pm3}$
		SEA (GIES)	**0.94**	1.2$_{\pm1}$	**0.88**	2.6$_{\pm4}$	**0.93**	3.2$_{\pm1}$	**0.84**	4.0$_{\pm3}$	**0.79**	**5.8**$_{\pm3}$
10	40	DCDI-G	0.50	19.8$_{\pm2}$	0.64	17.4$_{\pm3}$	0.82	8.0$_{\pm2}$	0.25	30.8$_{\pm4}$	0.23	31.0$_{\pm2}$
		DCDI-DSF	0.48	19.8$_{\pm3}$	0.55	21.6$_{\pm7}$	0.87	**6.0**$_{\pm3}$	0.25	31.4$_{\pm3}$	0.25	30.0$_{\pm3}$
		DCD-FG	0.35	28.6$_{\pm4}$	0.40	26.0$_{\pm1}$	0.36	26.8$_{\pm4}$	0.45	24.4$_{\pm5}$	0.41	25.5$_{\pm4}$
		DiffAn	0.41	27.6$_{\pm4}$	0.29	33.4$_{\pm4}$	0.49	26.4$_{\pm4}$	0.38	29.4$_{\pm6}$	0.32	31.8$_{\pm4}$
		DECI	0.43	27.6$_{\pm5}$	0.55	22.4$_{\pm4}$	0.50	25.4$_{\pm3}$	0.54	**21.5**$_{\pm3}$	0.57	**18.4**$_{\pm3}$
		AVICI	0.44	33.0$_{\pm5}$	0.68	28.4$_{\pm7}$	0.85	20.0$_{\pm4}$	0.50	35.0$_{\pm3}$	0.50	38.8$_{\pm2}$
		VarSort*	0.76	21.8$_{\pm5}$	0.81	15.4$_{\pm4}$	0.61	24.0$_{\pm4}$	0.67	33.6$_{\pm5}$	0.46	37.6$_{\pm2}$
		InvCov	—	40.2$_{\pm2}$	—	44.6$_{\pm2}$	—	41.0$_{\pm3}$	—	44.2$_{\pm3}$	—	42.3$_{\pm2}$
		FCI*	0.16	39.2$_{\pm2}$	0.24	38.8$_{\pm3}$	0.22	36.2$_{\pm3}$	0.22	38.8$_{\pm2}$	0.16	39.9$_{\pm2}$
		GIES*	0.44	33.4$_{\pm4}$	0.60	33.0$_{\pm5}$	0.51	32.0$_{\pm3}$	0.38	36.7$_{\pm2}$	0.63	34.6$_{\pm3}$
		SEA (FCI)	0.80	18.6$_{\pm2}$	0.89	15.4$_{\pm4}$	0.87	18.8$_{\pm4}$	0.78	24.4$_{\pm6}$	0.69	26.9$_{\pm4}$
		SEA (GIES)	**0.91**	**12.8**$_{\pm4}$	**0.95**	**10.4**$_{\pm6}$	**0.89**	17.2$_{\pm3}$	**0.87**	24.5$_{\pm3}$	**0.93**	29.5$_{\pm3}$
20	20	DCDI-G	0.75	6.4$_{\pm2}$	0.90	**3.0**$_{\pm2}$	0.84	**4.4**$_{\pm2}$	0.39	42.7$_{\pm6}$	0.48	10.4$_{\pm3}$
		DCDI-DSF	0.77	5.2$_{\pm3}$	0.85	4.2$_{\pm4}$	0.64	11.6$_{\pm3}$	0.41	43.2$_{\pm6}$	0.45	15.7$_{\pm5}$
		DCD-FG	0.76	51.2$_{\pm12}$	0.88	177$_{\pm57}$	0.85	193$_{\pm27}$	0.65	251$_{\pm35}$	0.60	52.7$_{\pm19}$
		DiffAn	0.56	40.2$_{\pm27}$	0.47	38.6$_{\pm26}$	0.53	35.0$_{\pm26}$	0.63	19.2$_{\pm8}$	0.42	49.7$_{\pm15}$
		DECI	0.54	52.0$_{\pm17}$	0.56	41.0$_{\pm14}$	0.56	39.0$_{\pm8}$	0.65	30.0$_{\pm9}$	0.73	18.9$_{\pm6}$
		AVICI	0.56	17.2$_{\pm5}$	0.69	10.8$_{\pm2}$	0.79	11.2$_{\pm3}$	0.53	17.2$_{\pm5}$	0.37	18.4$_{\pm4}$
		VarSort*	0.84	10.0$_{\pm3}$	0.88	6.6$_{\pm6}$	0.74	14.6$_{\pm8}$	0.50	16.1$_{\pm4}$	0.40	17.1$_{\pm4}$
		InvCov	—	23.6$_{\pm6}$	—	24.6$_{\pm5}$	—	24.6$_{\pm6}$	—	22.9$_{\pm5}$	—	20.0$_{\pm5}$
		FCI*	0.70	19.0$_{\pm5}$	0.45	17.4$_{\pm2}$	0.50	19.4$_{\pm6}$	0.57	18.5$_{\pm4}$	0.44	18.9$_{\pm5}$
		GIES*	0.80	7.4$_{\pm2}$	0.77	9.0$_{\pm5}$	0.71	14.0$_{\pm3}$	0.75	12.5$_{\pm4}$	0.68	13.7$_{\pm4}$
		SEA (FCI)	**0.92**	3.2$_{\pm3}$	0.93	5.0$_{\pm3}$	0.94	8.8$_{\pm3}$	0.79	**6.7**$_{\pm3}$	0.76	**9.8**$_{\pm4}$
		SEA (GIES)	0.89	**3.0**$_{\pm1}$	**0.95**	3.4$_{\pm2}$	**0.94**	7.8$_{\pm3}$	**0.83**	8.1$_{\pm3}$	**0.78**	10.1$_{\pm4}$
20	80	DCDI-G	0.54	44.0$_{\pm6}$	0.53	61.6$_{\pm11}$	0.89	37.4$_{\pm34}$	0.46	44.2$_{\pm5}$	0.26	59.7$_{\pm5}$
		DCDI-DSF	0.57	41.2$_{\pm3}$	0.61	**60.0**$_{\pm12}$	0.85	**28.4**$_{\pm26}$	0.47	43.6$_{\pm6}$	0.30	57.6$_{\pm5}$
		DCD-FG	0.58	172$_{\pm27}$	0.65	156$_{\pm41}$	0.75	162$_{\pm49}$	0.62	80.1$_{\pm13}$	0.48	79.8$_{\pm7}$
		DiffAn	0.46	127$_{\pm5}$	0.28	154$_{\pm10}$	0.36	145$_{\pm7}$	0.45	117$_{\pm21}$	0.21	157$_{\pm7}$
		DECI	0.30	87.2$_{\pm3}$	0.47	104$_{\pm7}$	0.35	79.6$_{\pm9}$	0.48	71.0$_{\pm7}$	0.57	58.9$_{\pm11}$
		AVICI	0.51	75.6$_{\pm10}$	0.69	72.8$_{\pm6}$	0.69	61.2$_{\pm10}$	0.50	70.6$_{\pm6}$	0.50	75.5$_{\pm7}$
		VarSort*	0.82	44.8$_{\pm4}$	0.84	73.6$_{\pm13}$	0.61	65.2$_{\pm10}$	0.67	63.4$_{\pm5}$	0.39	75.6$_{\pm5}$
		InvCov	—	97.6$_{\pm6}$	—	121$_{\pm4}$	—	104$_{\pm9}$	—	95.6$_{\pm7}$	—	97.8$_{\pm4}$
		FCI*	0.19	75.8$_{\pm11}$	0.19	80.2$_{\pm5}$	0.22	74.4$_{\pm8}$	0.33	72.3$_{\pm6}$	0.23	76.6$_{\pm5}$
		GIES*	0.56	70.0$_{\pm11}$	0.73	75.2$_{\pm4}$	0.59	67.4$_{\pm7}$	0.62	65.6$_{\pm7}$	0.61	68.1$_{\pm5}$
		SEA (FCI)	0.86	39.8$_{\pm12}$	0.87	73.8$_{\pm12}$	**0.92**	52.0$_{\pm9}$	0.82	**42.9**$_{\pm6}$	0.69	**57.0**$_{\pm5}$
		SEA (GIES)	**0.92**	**26.8**$_{\pm8}$	**0.88**	71.4$_{\pm8}$	**0.92**	50.6$_{\pm7}$	**0.84**	45.0$_{\pm7}$	**0.89**	60.1$_{\pm6}$

Table 19: Full results on synthetic datasets (continuous metrics). Mean over 5 distinct scale-free graphs. † indicates o.o.d setting. ∗ indicates non-parametric bootstrapping. All standard deviations were within 0.02.

N	E	Model	Linear		NN add.		NN non-add.		Sigmoid†		Polynomial†	
			mAP ↑	AUC ↑	mAP ↑	AUC ↑	mAP ↑	AUC ↑	mAP ↑	AUC ↑	mAP ↑	AUC ↑
10	10	Dcdi-G	0.54	0.90	0.59	0.88	0.69	0.89	0.48	0.77	0.50	0.73
		Dcdi-Dsf	0.70	0.92	0.71	0.88	0.36	0.83	0.46	0.75	0.49	0.76
		Dcd-Fg	0.56	0.76	0.47	0.72	0.50	0.73	0.44	0.68	0.57	0.75
		DiffAn	0.25	0.73	0.15	0.66	0.16	0.62	0.31	0.75	0.24	0.63
		Deci	0.17	0.65	0.17	0.67	0.20	0.72	0.27	0.73	0.49	0.82
		Avici	0.51	0.87	0.55	0.85	0.76	0.95	0.44	0.81	0.27	0.71
		VarSort*	0.67	0.84	0.69	0.86	0.76	0.88	0.45	0.69	0.46	0.73
		InvCov	0.50	0.92	0.41	0.87	0.38	0.84	0.47	0.90	0.45	0.86
		Fci*	0.56	0.80	0.51	0.80	0.43	0.74	0.60	0.82	0.34	0.68
		Gies*	0.87	0.98	0.61	0.94	0.69	0.94	0.75	0.96	0.71	**0.91**
		Sea (Fci)	**0.96**	**0.99**	0.88	0.98	0.88	0.97	0.79	0.96	0.73	0.90
		Sea (Gies)	0.95	**0.99**	**0.94**	**0.98**	**0.92**	**0.98**	**0.85**	**0.98**	**0.74**	0.90
10	40	Dcdi-G	0.70	0.85	0.74	0.85	**0.88**	**0.91**	0.56	0.66	0.53	0.64
		Dcdi-Dsf	0.74	0.87	0.73	0.84	0.71	0.90	0.56	0.69	0.51	0.63
		Dcd-Fg	0.37	0.58	0.45	0.61	0.45	0.58	0.49	0.63	0.63	0.73
		DiffAn	0.29	0.50	0.25	0.38	0.28	0.46	0.31	0.53	0.27	0.44
		Deci	0.30	0.51	0.41	0.65	0.33	0.51	0.38	0.60	0.59	0.77
		Avici	0.41	0.57	0.65	0.81	0.55	0.67	0.41	0.59	0.40	0.61
		VarSort*	0.77	0.83	0.74	0.87	0.59	0.71	0.66	0.76	0.50	0.66
		InvCov	0.44	0.71	0.38	0.59	0.42	0.62	0.44	0.67	0.42	0.62
		Fci*	0.47	0.64	0.41	0.60	0.40	0.58	0.48	0.64	0.41	0.59
		Gies*	0.43	0.68	0.43	0.63	0.44	0.61	0.49	0.69	0.59	0.71
		Sea (Fci)	0.85	0.91	0.80	0.90	0.77	0.88	0.76	0.83	0.66	0.71
		Sea (Gies)	**0.92**	**0.96**	**0.84**	**0.93**	0.83	0.90	**0.79**	**0.88**	**0.78**	**0.87**
20	20	Dcdi-G	0.41	0.95	0.50	0.94	0.69	0.96	0.37	0.83	0.37	0.77
		Dcdi-Dsf	0.48	0.95	0.55	0.93	0.33	0.90	0.37	0.79	0.35	0.82
		Dcd-Fg	0.51	0.87	0.39	0.83	0.48	0.84	0.56	0.84	0.50	0.84
		DiffAn	0.27	0.80	0.11	0.65	0.11	0.66	0.26	0.77	0.12	0.69
		Deci	0.13	0.69	0.15	0.71	0.15	0.73	0.15	0.71	0.25	0.79
		Avici	0.53	0.88	0.66	0.89	0.74	0.92	0.46	0.87	0.32	0.77
		VarSort*	0.67	0.85	0.84	0.93	0.59	0.86	0.45	0.72	0.44	0.73
		InvCov	0.44	0.94	0.35	0.91	0.30	0.89	0.43	0.93	0.41	0.87
		Fci*	0.63	0.84	0.44	0.78	0.43	0.79	0.60	0.86	0.47	0.78
		Gies*	0.82	0.99	0.58	0.95	0.57	0.96	0.75	0.98	0.61	0.90
		Sea (Fci)	**0.94**	**1.00**	0.87	**0.98**	0.83	0.97	**0.82**	**0.98**	**0.72**	**0.92**
		Sea (Gies)	0.93	**1.00**	**0.91**	0.98	**0.88**	**0.98**	**0.82**	0.98	0.70	0.91
20	80	Dcdi-G	0.62	0.88	0.61	**0.89**	**0.76**	**0.94**	0.44	0.76	0.36	0.60
		Dcdi-Dsf	0.58	0.87	0.55	0.86	0.58	0.92	0.43	0.78	0.35	0.66
		Dcd-Fg	0.38	0.70	0.30	0.69	0.48	0.80	0.48	0.75	0.53	0.73
		DiffAn	0.18	0.55	0.15	0.44	0.16	0.53	0.19	0.56	0.15	0.38
		Deci	0.21	0.58	0.24	0.64	0.26	0.66	0.30	0.68	0.41	0.75
		Avici	0.29	0.61	0.54	0.80	0.60	0.85	0.35	0.65	0.28	0.63
		VarSort*	0.79	0.90	0.57	0.83	0.62	0.81	0.57	0.77	0.38	0.64
		InvCov	0.38	0.81	0.22	0.56	0.32	0.73	0.38	0.78	0.33	0.67
		Fci*	0.31	0.63	0.30	0.62	0.30	0.62	0.41	0.68	0.32	0.62
		Gies*	0.51	0.87	0.43	0.78	0.47	0.81	0.52	0.82	0.47	0.73
		Sea (Fci)	0.87	0.96	0.59	0.87	0.70	0.90	0.73	0.87	0.53	0.71
		Sea (Gies)	**0.92**	**0.98**	**0.63**	0.89	0.73	0.91	**0.77**	**0.92**	**0.62**	**0.84**

Table 20: Full results on synthetic datasets (discrete metrics). Mean/std over 5 distinct scale-free graphs. † indicates o.o.d. setting. $\ast$ indicates non-parametric bootstrapping. All OA standard deviations within 0.2.

N	E	Model	Linear		NN add.		NN non-add.		Sigmoid†		Polynomial†	
			OA ↑	SHD ↓	OA ↑	SHD ↓	OA ↑	SHD ↓	OA ↑	SHD ↓	OA ↑	SHD ↓
10	10	Dcdi-G	0.51	16.6$_{\pm 1}$	0.61	17.4$_{\pm 2}$	0.71	16.2$_{\pm 2}$	0.59	16.9$_{\pm 5}$	0.63	16.6$_{\pm 3}$
		Dcdi-Dsf	0.70	16.2$_{\pm 2}$	0.75	15.4$_{\pm 3}$	0.36	16.8$_{\pm 2}$	0.48	18.1$_{\pm 3}$	0.67	18.0$_{\pm 2}$
		Dcd-Fg	0.60	16.4$_{\pm 5}$	0.57	22.2$_{\pm 4}$	0.57	20.0$_{\pm 4}$	0.47	17.9$_{\pm 4}$	0.59	16.8$_{\pm 5}$
		DiffAn	0.55	9.2$_{\pm 4}$	0.49	14.6$_{\pm 4}$	0.36	11.6$_{\pm 4}$	0.59	7.7$_{\pm 4}$	0.42	14.8$_{\pm 6}$
		Deci	0.51	17.4$_{\pm 5}$	0.55	17.4$_{\pm 5}$	0.58	12.0$_{\pm 2}$	0.62	12.6$_{\pm 5}$	0.74	8.2$_{\pm 6}$
		Avici	0.64	6.8$_{\pm 3}$	0.59	5.4$_{\pm 3}$	0.77	3.6$_{\pm 1}$	0.48	7.8$_{\pm 3}$	0.35	9.5$_{\pm 3}$
		VarSort*	0.82	4.4$_{\pm 1}$	0.78	4.8$_{\pm 2}$	0.80	3.4$_{\pm 2}$	0.47	7.3$_{\pm 3}$	0.55	8.1$_{\pm 3}$
		InvCov	—	8.8$_{\pm 3}$	—	9.2$_{\pm 2}$	—	9.8$_{\pm 1}$	—	9.7$_{\pm 3}$	—	10.2$_{\pm 2}$
		Fci*	0.62	8.4$_{\pm 2}$	0.51	7.8$_{\pm 2}$	0.45	8.0$_{\pm 2}$	0.61	9.2$_{\pm 3}$	0.34	9.6$_{\pm 2}$
		Gies*	0.83	2.2$_{\pm 2}$	0.60	6.0$_{\pm 2}$	0.75	4.2$_{\pm 2}$	0.72	4.9$_{\pm 3}$	0.73	5.7$_{\pm 2}$
		Sea (Fci)	**0.89**	**1.4**$_{\pm 2}$	0.90	2.6$_{\pm 2}$	0.93	2.2$_{\pm 1}$	0.71	4.0$_{\pm 3}$	0.72	5.2$_{\pm 2}$
		Sea (Gies)	0.85	**1.4**$_{\pm 1}$	**0.96**	**1.8**$_{\pm 1}$	**0.94**	**2.0**$_{\pm 1}$	**0.86**	**3.4**$_{\pm 3}$	**0.83**	**5.0**$_{\pm 2}$
10	40	Dcdi-G	0.82	24.0$_{\pm 4}$	0.85	27.8$_{\pm 5}$	0.87	19.6$_{\pm 2}$	0.62	31.4$_{\pm 3}$	0.52	32.6$_{\pm 4}$
		Dcdi-Dsf	0.79	22.8$_{\pm 5}$	0.79	24.4$_{\pm 4}$	0.82	20.4$_{\pm 2}$	0.64	31.6$_{\pm 2}$	0.58	33.3$_{\pm 3}$
		Dcd-Fg	0.36	24.8$_{\pm 4}$	0.41	25.2$_{\pm 5}$	0.38	25.6$_{\pm 8}$	0.41	23.2$_{\pm 6}$	0.54	18.5$_{\pm 3}$
		DiffAn	0.40	29.8$_{\pm 8}$	0.28	37.0$_{\pm 2}$	0.38	32.6$_{\pm 2}$	0.45	28.0$_{\pm 6}$	0.33	32.7$_{\pm 5}$
		Deci	0.43	27.8$_{\pm 3}$	0.66	22.6$_{\pm 3}$	0.48	28.6$_{\pm 3}$	0.52	22.2$_{\pm 4}$	0.66	**13.3**$_{\pm 3}$
		Avici	0.43	20.2$_{\pm 4}$	0.84	17.2$_{\pm 4}$	0.61	20.4$_{\pm 8}$	0.52	24.8$_{\pm 3}$	0.49	26.5$_{\pm 2}$
		VarSort*	0.75	13.4$_{\pm 2}$	0.89	**12.6**$_{\pm 2}$	0.60	20.6$_{\pm 3}$	0.65	20.8$_{\pm 4}$	0.50	26.4$_{\pm 2}$
		InvCov	—	31.4$_{\pm 3}$	—	37.2$_{\pm 4}$	—	36.0$_{\pm 4}$	—	32.3$_{\pm 5}$	—	34.8$_{\pm 3}$
		Fci*	0.33	23.8$_{\pm 2}$	0.28	27.2$_{\pm 2}$	0.25	27.6$_{\pm 4}$	0.36	26.1$_{\pm 2}$	0.24	27.3$_{\pm 2}$
		Gies*	0.46	21.8$_{\pm 3}$	0.50	24.4$_{\pm 2}$	0.48	25.2$_{\pm 5}$	0.52	22.7$_{\pm 3}$	0.64	22.5$_{\pm 2}$
		Sea (Fci)	0.80	10.0$_{\pm 4}$	0.88	14.0$_{\pm 2}$	0.87	15.8$_{\pm 3}$	0.79	15.6$_{\pm 3}$	0.64	18.5$_{\pm 3}$
		Sea (Gies)	**0.88**	**6.6**$_{\pm 3}$	**0.98**	14.0$_{\pm 5}$	**0.88**	**14.4**$_{\pm 3}$	**0.87**	**14.1**$_{\pm 3}$	**0.93**	19.1$_{\pm 3}$
20	20	Dcdi-G	0.54	40.4$_{\pm 2}$	0.70	44.8$_{\pm 8}$	0.88	39.8$_{\pm 6}$	0.47	41.1$_{\pm 4}$	0.53	38.4$_{\pm 6}$
		Dcdi-Dsf	0.64	40.4$_{\pm 3}$	0.65	42.4$_{\pm 8}$	0.40	42.2$_{\pm 8}$	0.37	41.1$_{\pm 4}$	0.45	49.3$_{\pm 18}$
		Dcd-Fg	0.68	252$_{\pm 23}$	0.77	183$_{\pm 52}$	0.78	181$_{\pm 27}$	0.70	251$_{\pm 45}$	0.69	278$_{\pm 68}$
		DiffAn	0.67	23.6$_{\pm 13}$	0.40	42.2$_{\pm 22}$	0.42	34.0$_{\pm 11}$	0.59	22.6$_{\pm 12}$	0.50	46.8$_{\pm 13}$
		Deci	0.50	42.0$_{\pm 5}$	0.54	43.0$_{\pm 11}$	0.57	40.0$_{\pm 13}$	0.51	34.7$_{\pm 7}$	0.65	25.3$_{\pm 6}$
		Avici	0.68	11.8$_{\pm 3}$	0.79	9.2$_{\pm 2}$	0.80	7.8$_{\pm 2}$	0.60	15.3$_{\pm 4}$	0.45	18.3$_{\pm 5}$
		VarSort*	0.74	10.4$_{\pm 3}$	0.91	6.2$_{\pm 2}$	0.76	13.0$_{\pm 6}$	0.49	13.7$_{\pm 4}$	0.51	16.7$_{\pm 6}$
		InvCov	—	20.2$_{\pm 3}$	—	24.4$_{\pm 5}$	—	23.8$_{\pm 5}$	—	21.2$_{\pm 4}$	—	20.8$_{\pm 5}$
		Fci*	0.67	13.8$_{\pm 2}$	0.52	17.4$_{\pm 1}$	0.53	17.8$_{\pm 5}$	0.65	16.7$_{\pm 4}$	0.50	18.9$_{\pm 5}$
		Gies*	0.82	6.4$_{\pm 3}$	0.71	12.6$_{\pm 2}$	0.68	13.2$_{\pm 3}$	0.75	11.4$_{\pm 5}$	0.73	13.4$_{\pm 4}$
		Sea (Fci)	**0.90**	**2.8**$_{\pm 1}$	0.87	7.0$_{\pm 2}$	0.91	8.2$_{\pm 5}$	0.73	**7.7**$_{\pm 3}$	0.71	**9.5**$_{\pm 4}$
		Sea (Gies)	0.85	4.0$_{\pm 2}$	**0.95**	**3.6**$_{\pm 2}$	**0.93**	**6.2**$_{\pm 4}$	**0.80**	7.9$_{\pm 4}$	**0.82**	9.9$_{\pm 3}$
20	80	Dcdi-G	0.81	93.0$_{\pm 10}$	0.73	104$_{\pm 7}$	**0.91**	67.8$_{\pm 8}$	0.61	82.5$_{\pm 8}$	0.53	79.7$_{\pm 5}$
		Dcdi-Dsf	0.75	103$_{\pm 7}$	0.73	94.8$_{\pm 11}$	0.77	63.8$_{\pm 7}$	0.65	84.4$_{\pm 8}$	0.52	82.6$_{\pm 5}$
		Dcd-Fg	0.63	188$_{\pm 24}$	0.70	187$_{\pm 14}$	0.78	190$_{\pm 26}$	0.71	217$_{\pm 38}$	0.71	235$_{\pm 32}$
		DiffAn	0.42	111$_{\pm 18}$	0.30	145$_{\pm 11}$	0.40	119$_{\pm 13}$	0.41	100$_{\pm 22}$	0.21	149$_{\pm 11}$
		Deci	0.33	72.2$_{\pm 10}$	0.48	81.4$_{\pm 10}$	0.48	67.0$_{\pm 9}$	0.50	60.4$_{\pm 12}$	0.58	**47.2**$_{\pm 7}$
		Avici	0.45	56.0$_{\pm 5}$	0.77	**47.6**$_{\pm 8}$	0.76	42.6$_{\pm 3}$	0.50	54.0$_{\pm 6}$	0.47	62.2$_{\pm 5}$
		VarSort*	0.85	32.4$_{\pm 5}$	0.84	54.8$_{\pm 8}$	0.75	40.2$_{\pm 6}$	0.64	54.0$_{\pm 6}$	0.37	60.1$_{\pm 5}$
		InvCov	—	79.4$_{\pm 6}$	—	106$_{\pm 5}$	—	87.4$_{\pm 2}$	—	78.8$_{\pm 9}$	—	86.2$_{\pm 4}$
		Fci*	0.26	58.2$_{\pm 6}$	0.22	58.4$_{\pm 4}$	0.26	55.0$_{\pm 7}$	0.37	59.3$_{\pm 6}$	0.23	62.9$_{\pm 4}$
		Gies*	0.65	48.4$_{\pm 5}$	0.71	53.6$_{\pm 3}$	0.68	48.0$_{\pm 4}$	0.64	53.6$_{\pm 6}$	0.61	54.9$_{\pm 5}$
		Sea (Fci)	0.91	25.6$_{\pm 6}$	0.88	51.6$_{\pm 6}$	0.89	42.2$_{\pm 4}$	0.83	36.1$_{\pm 6}$	0.71	47.4$_{\pm 5}$
		Sea (Gies)	**0.92**	**17.6**$_{\pm 3}$	**0.93**	49.2$_{\pm 9}$	0.89	**37.2**$_{\pm 5}$	**0.88**	**35.1**$_{\pm 7}$	**0.89**	48.1$_{\pm 5}$

Table 21: Causal discovery results on synthetic datasets with 100 nodes, continuous metrics. Each setting encompasses 5 distinct Erdős-Rényi graphs. The symbol † indicates that the model was not trained on this setting. All standard deviations were within 0.1.

N	E	Model	Linear		NN add.		NN non-add.		Sigmoid†		Polynomial†	
			mAP ↑	AUC ↑	mAP ↑	AUC ↑	mAP ↑	AUC ↑	mAP ↑	AUC ↑	mAP ↑	AUC ↑
100	100	Dcd-Fg	0.11	0.75	0.12	0.71	0.18	0.73	0.20	0.72	0.06	0.60
		InvCov	0.40	0.99	0.22	0.94	0.16	0.87	0.40	0.97	0.36	0.90
		Sea (Fci)	0.96	1.00	0.83	0.97	0.75	0.97	0.79	0.97	0.56	0.88
		Sea (Gies)	0.97	1.00	0.82	0.98	0.74	0.96	0.80	0.97	0.54	0.85
100	400	Dcd-Fg	0.05	0.59	0.07	0.64	0.10	0.72	0.13	0.72	0.12	0.64
		InvCov	0.25	0.91	0.09	0.62	0.14	0.77	0.27	0.86	0.20	0.67
		Sea (Fci)	0.90	0.99	0.28	0.82	0.60	0.92	0.69	0.92	0.38	0.80
		Sea (Gies)	0.91	0.99	0.27	0.82	0.61	0.92	0.69	0.91	0.38	0.78

Table 22: Causal discovery results on synthetic datasets with 100 nodes, discrete metrics. Each setting encompasses 5 distinct Erdős-Rényi graphs. The symbol † indicates that the model was not trained on this setting.

N	E	Model	Linear		NN add.		NN non-add.		Sigmoid†		Polynomial†	
			OA ↑	SHD ↓	OA ↑	SHD ↓	OA ↑	SHD ↓	OA ↑	SHD ↓	OA ↑	SHD ↓
100	100	Dcd-Fg	0.63	3075.8	0.58	2965.0	0.60	2544.4	0.59	3808.0	0.34	1927.9
		InvCov	—	124.4	—	130.0	—	158.8	—	112.3	—	106.3
		Sea (Fci)	0.91	13.4	0.90	34.4	0.91	47.2	0.78	40.3	0.69	59.2
		Sea (Gies)	0.91	13.6	0.93	32.8	0.91	45.8	0.78	38.6	0.68	60.3
100	400	Dcd-Fg	0.46	3068.2	0.60	3428.8	0.70	3510.8	0.67	3601.8	0.53	3316.7
		InvCov	—	557.0	—	667.8	—	639.0	—	514.7	—	539.4
		Sea (Fci)	0.93	122.0	0.90	361.2	0.91	273.2	0.87	226.9	0.82	327.0
		Sea (Gies)	0.94	116.6	0.91	364.4	0.92	266.8	0.87	218.3	0.84	328.0

Table 23: Complete results on Sachs flow cytometry dataset (Sachs et al., 2005), using the subset proposed by (Wang et al., 2017).

Model	mAP ↑	AUC ↑	SHD ↓
DCDI-G	0.17	0.55	21
DCDI-DSF	0.20	0.59	20
DCD-FG	0.32	0.59	27
DIFFAN	0.14	0.45	37
DECI	0.21	0.62	28
AVICI-L	0.35	0.78	20
AVICI-R	0.29	0.65	18
AVICI-L+R	**0.59**	**0.83**	14
FCI*	0.27	0.59	18
GIES*	0.21	0.59	17
SEA (FCI)	0.23	0.54	24
+KCI	0.33	0.63	14
+CORR	0.41	0.70	15
+KCI+CORR	0.49	0.71	**13**
SEA (GIES)	0.23	0.60	14